Springer Handbooks

Springer Handbook of Crystal Growth

Bearbeitet von
Govindhan Dhanaraj, Kullaiah Byrappa, Vishwanath Prasad, Michael Dudley

1. Auflage 2010. Buch. XXXVIII, 1818 S.
ISBN 978 3 540 74182 4
Format (B x L): 19,3 x 24,2 cm

4. Generation and Propagation of Defects During Crystal Growth

Helmut Klapper

This chapter presents a review of the typical growth defects of crystals fully grown on (planar) habit faces, i. e. of crystals grown in all kinds of solutions, in supercooled melt (mainly low-melting organics) and in the vapour phase. To a smaller extent also growth on rounded faces from the melt is considered when it seemed to be adequate to bring out analogies or discuss results in a more general context. The origins and the typical configurations of defects developing *during* growth and *after* growth are illustrated by a series of selected x-ray diffraction topographs (Lang technique) and, in a few cases, by optical photographs.

After the introduction (Sect. 4.1) the review starts with the formation of inclusions (Sect. 4.2) which are the main origin of other growth defects such as dislocations and twins. Three kinds of inclusions are treated: foreign particles, liquid inclusions (of nutrient solution) and solute precipitates. Particular attention is directed to the regeneration of seed crystals into a fully facetted shape (*capping*), and inclusion formation due to improper hydrodynamics in the solution (especially for KDP).

Section 4.3 deals shortly with striations (treated in more detail in another Chapter) and more comprehensive with the different kinds of crystal regions grown on different growth faces: growth sectors, vicinal sectors, facet sectors. These regions are usually differently perfect and possess more or less different physical properties, and the boundaries between them frequently are faulted internal surfaces of the crystal. Two subsections treat the optical anomalies of growth and vicinal sectors and the determination of the relative growth rates of neighboured growth faces from the orientation of their common sector boundary.

In Sect. 4.4 distinction is made between dislocations connected to and propagating with the growth interface (*growth dislocations*), and dislocations generated *behind* the growth front by plastic glide due to stress relaxation. The main sources of both types of dislocations are inclusions. In crystals grown on planar faces, growth dislocations are usually straight-lined and follow (frequently noncrystallographic) preferred directions depending on the Burgers vector, on the growth direction and the elastic constants of the crystal. These directions are explained by a minimum of the dislocation line energy per growth length or, equivalently, by zero force exerted by the growth surface on the dislocation. Calculations based on anisotropic linear elasticity of a continuum confirm this approach. The influence of the discrete lattice structure and core energy on dislocation directions is discussed. Further subsections deal with the Burgers vector determination by preferred directions, with the post-growth movement of grown-in dislocations, with the generation of post-growth dislocations, and with the growth-promoting effect of edge dislocations.

In Sect. 4.5, *Twinning*, the main characteristics of twins and their boundaries, their generation by nucleation and by inclusions, their propagation with the growth front and their growth promoting effect are presented. The post-growth formation of twins by phase transitions and ferroelastic (mechanical) switching is shortly outlined. The last Sect. 4.6 compares the perfection of crystals (KDP and ADP) slowly and rapidly grown from solutions, that the optical and structural quality of rapidly grown crystals is not inferior to that of slowly grown crystals, if particular precautions and growth conditions are met.

4.1 Overview

The present chapter mainly deals with growth defects in crystals fully grown on (planar) habit faces. To a smaller extent also crystals grown on rounded faces from the melt are considered when it seemed to be adequate to bring out analogies or discuss results in a more general context. Crystals grow on habit faces in solutions, in supercooled melts and in the vapour. A special feature of this growth method is that there is practically no temperature gradient inside the crystal, provided that facet growth occurs freely on the whole surface of the crystal (without contact to a container wall). This is also the case for growth in the supercooled melt: the crystallization heat released at the growing habit faces keeps these on crystallization temperature – or at least close to it [4.1]. The absence of a temperature gradient and, thus, of thermal stress inside the crystal allows the development of defect structures according to first thermodynamical principles and to preserve them in their as-grown geometries, unless thermal gradients are introduced by improper cooling to room temperature after growth. This particularly concerns dislocations in crystals growing in their plastic state. Dislocations are the essential elements of stress relaxation by plastic glide: they are generated, moved and multiplied by stress. Thus – in the presence of thermal stress – it makes an essential difference whether crystals are grown in their brittle or their plastic state. From solution, crystals grow in the brittle or in the plastic state (dependent on the specific mechanical properties at growth temperature); from the melt, however, crystals *always* grow in the plastic state, because each material has a more or less extended plastic zone below its melting point. It will be shown that growth dislocations develop the same geometrical features in crystals grown on habit faces from solution in the brittle state and from supercooled melts in the plastic state, provided thermal gradients are absent.

In this review the generation of defects at the interface and the propagation with the advancing growth front are separately considered. This is because certain defects formed by a growth disturbance (e.g. by inclusions) may *heal out* and do not continue into the further growing crystal, whereas other defects (dislocations, twins, grain boundaries), once initiated, are *forced* to proceed with the interface despite growth under optimal conditions. These defects can only be eliminated by growing out at the sides of the crystal, e.g., during Czochralski pulling on interfaces which are convex toward the melt. Moreover, distinction is made between *defects always connected to the interface* (*growth defects,* esp. *growth dislocations*) and *defects generated 'behind' the growth front* (*post-growth defects*). The latter defects may be formed already during the growth run, either by thermal stress or by precipitation. Furthermore, defect configurations may be preserved in their *as-grown* geometry or changed after growth (e.g., *post-growth* movement of dislocations).

Many experimental results and the majority of photographs presented in this review were obtained by growth experiments and x-ray topographic studies

(Lang technique) in the author's laboratories in Aachen and Bonn. Crystals were grown from aqueous and organic solutions, from supercooled melts (organics) and by Czochralski pulling (organics). The organic crystals were considered as low-melting *model substances* (melting points below 100 °C), chosen with the primary aim to study the generation and propagation of growth defects in dependence on growth methods and varying growth conditions. The main characterisation method, x-ray diffraction topography, is not treated here; the reader is referred to the reviews [4.2–5] in the literature and to Chap. XX chap]Please supply the chapter title or number. by *Dudley* in this Handbook. More specialized x-ray topographic treatments are given for twinned crystals [4.6] and for organic crystals [4.7]. Earlier reviews on the generation and propagation of growth defects were published by the author [4.8–11].

4.2 Inclusions

Two categories of inclusions are distinguished according their genetic origin [4.12, 13]: *primary inclusions* are associated with the growth front, i. e. they arise during growth, whereas *secondary inclusions* are formed after growth. Primary inclusions are *key defects* because they are the source of other defects (dislocations, twins) which propagate with the growth front into the further growing crystal. Inclusions of both categories may form stress centres which give rise to dislocation loops or half-loops by plastic glide (stress relaxation). Among primary inclusions three kinds are distinguished:

- Foreign particles
- Solvent (liquid) inclusions in crystals grown from solutions
- Solute precipitations in crystals grown from impure or doped melts

Secondary inclusions are precipitates of solute impurities (dopants) formed after growth in the solid state during slow cooling, annealing or processing of crystals which are grown at high temperatures. They are due to the supersaturation of solutes at temperatures below the temperature at which the crystal was grown. These solutes precipitate if their diffusion mobility is sufficiently high and not frozen-in (as is usually the case at room temperature). In the same way vacancies and self-interstitials may condense into dislocation loops and stacking faults, e.g. during processing silicon crystals for electronic applications (*swirl defects*, e.g. [4.14]).

Here we treat only primary inclusions. A very detailed theoretical and experimental treatment of the capture of inclusions during crystal growth is presented by *Chernov* and *Temkin* [4.15]. A similar study with particular consideration of crystallization pressure is reported by *Khaimov-Mal'kov* [4.16].

4.2.1 Foreign Particles

Foreign particles pre-existing in the nutrient (solution, melt) increase the risk of (heterogeneous) nucleation. Their incorporation into the growing crystal, however, is often considered as not very critical due to the crystallisation pressure [4.16] (*disjoining force* after *Chernov* and *Temkin* [4.15]) which repulses foreign particles from the growth interface. Nevertheless, particles coming into contact with the growth face may be incorporated, depending on the size and chemical/physical nature of the particles and on growth conditions such as stirring, growth rate, supersaturation [4.15]. For example, potassium alum crystals can be grown inclusion-free (as assessed by optical inspection and x-ray topography) from *old* (i. e. repeatedly used) unfiltered aqueous solutions containing many floating dust particles, provided that growth conditions (temperature control, stirring) are stable enough to avoid the formation of liquid inclusions (see below). On the other hand in crystals of benzil grown in *old* (repeatedly filled up) supercooled melts ($T_m = 96\,°C$), flocks of solid decomposition products floating in the melt are quite readily incorporated (unpublished observation by the author). In contrast to the solution growth of potassium alum, such benzil melts were not stirred, but thermal convection occurred due to the release of crystallization heat at the crystal surface [4.1]. In the latter case the incorporation seems to be favoured by the higher viscosity and the lower agitation of the nutrient phase, and probably also by the chemical similarity (carbon) of the particles to the growing crystal.

Foreign solid inclusions are very common in minerals. In laboratory and industrial crystal growth they usually play a minor role because they are easily avoided by filtering of the nutrient before growth. If solid inclusions appear during the growth run, e.g.,

as abrasives of the stirring device, continuous filtering is advised. This has been demonstrated by *Zaitseva* et al. [4.17] for the rapid growth of huge KDP and DKDPdef]Please define this abbreviation at first use. crystals with linear sizes up to 55 cm: continuous filtering during the whole growth run considerably increased the optical quality and laser damage threshold of these crystals.

The intentional incorporation of particle inclusions for the study of the generation of dislocations is reported in Sect. 4.4.2. The intentional inclusion of oil drops during crystallization from solutions was studied by *Kliia* and *Sokolova* [4.18].

4.2.2 Solvent Inclusions

Solvent inclusions are very common in crystals grown by all variants of solution growth (aqueous and organic solvents, flux). Two origins are distinguished.

Facetting (*Capping*) of Rounded Surfaces

In general crystals grow from solutions with planar faces (habit faces), whereby faces with low surface energy grow slowly and determine the final morphology of the crystal (*Wulff theorem* [4.19]). If surfaces are rounded, (e.g., of the seed crystal or after redissolution), during first growth, facets of habit faces and (between them) terraces of these faces are formed. The facets become larger and the terraced regions grow out until a single edge between the two habit faces engaged is formed, as shown in Fig. 4.1 (*Theorem of Herring* [4.20–23], see also *growth on spheres* [4.24][4.25, p.130]). The *healed-out* regions often have the shape of caps (*capping region*). The growth on terraced surfaces favours the entrapment of solvent inclusions which may lead in extreme cases to a spongy structure of the capping region. This usually happens during first growth on seed crystals which were rounded during a final etching

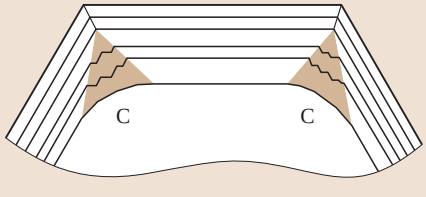

Fig. 4.1 Faceting and *capping* on rounded crystal surfaces. The shaded regions of terraced growth favour the entrapment of liquid inclusions. They grow out and finally form the growth-sector boundary between the main habit faces

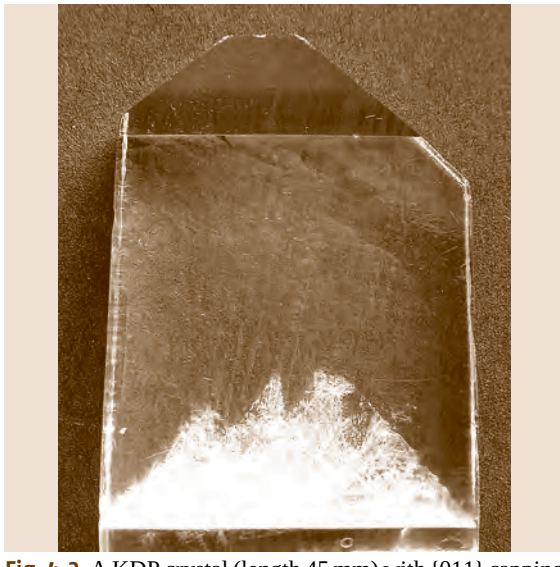

Fig. 4.2 A KDP crystal (length 45 mm) with {011} capping pyramid on a (001) seed plate

(which is necessary in order to remove surface impurities and defects) before seedingin. Therefore the zone of first growth around the seed crystals is usually more or less disturbed by liquid inclusions. These inclusions, however, can be largely avoided by a very slow (and thus time-consuming) growth under low supersaturation during the seed-faceting period.

A conspicuous example of capping is provided by potassium dihydrogen phosphate (KDP) grown in aqueous solution on (001) seed plates (Fig. 4.2). KDP develops habit faces {100} (tetragonal prism) and {101} (tetragonal dipyramid), but {001} is not a habit face. Thus in the first stage of growth on a (001) seed plate a spongy capping zone in the form of a tetragonal pyramid {101} over the seed plate as basis is formed, followed by clear further growth on {101} pyramid faces (Fig. 4.2). Detailed descriptions of this (001) capping process in KDP and ADP (ammonium dihydrogen phosphate) crystal growth are presented by *Zerfoss* and *Slawson* [4.12] and *Janssen-van Rosmalen* et al. [4.26].

Fluctuation of Growth Conditions (Growth Accidents)

A sufficiently strong change of growth condition (e.g., of supersaturation, stirring rate, stirring direction) may introduce – due to local variations of supersaturation – a (temporary) instability of growth faces: regions of retarded and promoted growth occur, leading to elevations and depressions on the growth face. Overhanging layers

and, thus, to changes of the impurity incorporation. As a rule, they affect the whole growth front and thus form inhomogeneity layers parallel to the interface. The term *striations* is usually applied when the impurity layers appear in a (quasi)-periodic sequence (Fig. 4.8a). If there are isolated layers, due to sporadic changes of growth conditions, often the term *growth bands* is used. In mineralogy, the notation *growth zoning* is common. In crystals grown under rotation, strictly periodic *rotational striations*, correlated with the rotation rate, may occur. They are due to a nonuniform radial temperature distribution around the rotation axis, leading to slight changes of growth conditions (even with remelting) within a rotation period.

The impurities may be contaminants of the solution or of the melt, or incorporated solvent components. Striations are also formed by dopants intentionally introduced with the aim to tailor specific physical properties of the crystals. The rate of incorporation depends on the species of impurities (dopants) and is governed by their distribution coefficient with regard to the crystal to be grown (see elsewhere in this Volume).

The regions of different impurities/dopants form layers coinciding with the instantaneous growth front. In crystals grown on habit faces (from solution or supercooled melt) they are planar as is shown in Figs. 4.8a and 4.9. The *intensity* of the striations, i. e. the concentration of impurities, may be considerably different in distinct growth sectors (see following Sect. 4.3.2). This is due to different surface structures of different growth faces which may facilitate or impede the impurity capture. Symmetrically equivalent growth sectors show the same *intensity* of striations unless the growth conditions (e.g., solution flow) at the corresponding growth faces are different. Conspicuous examples are the so-called hourglass growth patterns of crystals stained with organic dyes. *Staining of crystals* has been thoroughly studied by *Kahr* and *Guerney* [4.29], and *Kahr* and *Vasquez* [4.30]. Striations are often modified by growth hillocks (*vicinal pyramids*) as is shown below (Sect. 4.3.3). An x-ray topographic study of the striation formation in the presence of vicinal pyramids in rapidly grown KDP crystals is presented by *Smolsky* et al. [4.48].

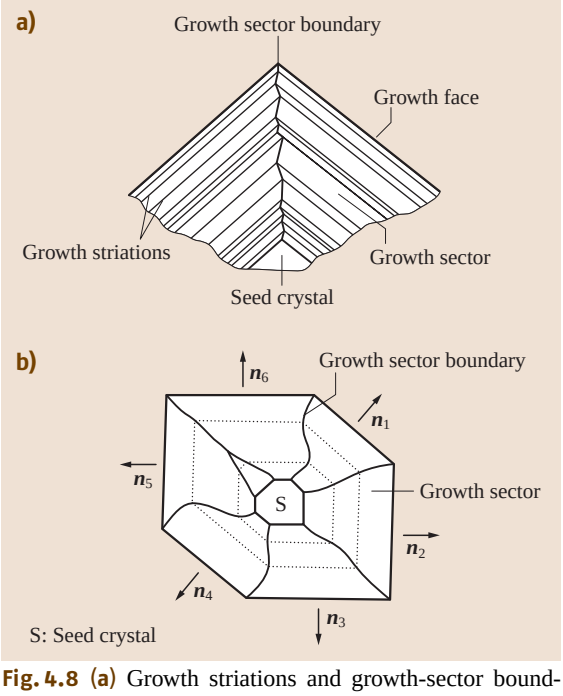

Fig. 4.8 (a) Growth striations and growth-sector boundary in a crystal grown on planar (habit) faces. The sector boundary is an internal surface formed by the movement of the edge joining the two faces during growth. It separates regions of different growth directions. (b) Division of a fully facetted crystal into growth sectors. The vectors $\boldsymbol{n}_i$ indicate the growth directions. *Dashed lines*: contours of the crystal at different stages of growth. One of the growth sectors has *grown out*

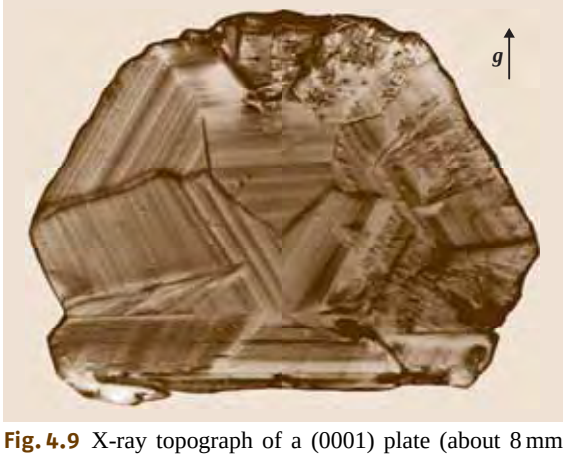

Fig. 4.9 X-ray topograph of a (0001) plate (about 8 mm diameter, 0.35 mm thick) cut out of a quartz-homeotypic gallium phosphate $GaPO_4$ crystal grown from high-temperature solution in phosphoric/sulphuric acid [4.47]. It shows the triangular arrangement of growth sectors with pronounced striations. Growth-sector boundaries are visible by topographic contrast or by the bends of the striations. Diffraction vector $\boldsymbol{g}(10\bar{1}0)$, AgK$\alpha$ radiation

Crystals grown on rounded interfaces exhibit curved striations. An example of striations accompanied by tiny gas bubbles in a Czochralski crystal is shown in Fig. 4.10. Facets formed on rounded interfaces lead to regions (*facet sectors*, Sect. 4.3.4 below) with planar striations. The occurrence and *intensity* of these striations may be quite different from striations formed along curved interfaces. This is due to distinct growth modes with different distribution coefficients for rough growth on curved interfaces and growth on facets from supercooled melt.

In general, growth striations lead to local changes of physical properties (e.g., electric conductivity, optical birefringence). This is a major problem in the growth of doped crystals for sophisticated electronic and optical solid-state devices. It can be encountered by the suppression of melt convection, e.g., by growth under microgravity [4.49] and by growth in magnetic fields [4.50], which are treated elsewhere in this Handbook. An extensive treatment of the origin of striations and of recipes to largely avoid them is presented by *Scheel* [4.51].

Fig. 4.10 Plate cut from the center of a Czochralski boule of orthorhombic salol ($T_m = 42\,°C$), about 1.3 mm thick, imaged length about 40 mm. The growth striations marking the interface at different stages of growth contain tiny gas bubbles, many of which are sources of growth dislocations. Due to the concave interface the dislocations are focussed toward the center of the boule. Due to this effect many dislocations enter the plate from above through the plate surface. Diffraction vector $\boldsymbol{g}(002)$, CuKα_1 radiation

4.3.2 Growth Sectors

Bulk crystals grow in all directions of space. Due to their structural and physical anisotropy, the types, distribution and geometry of growth defects are distinct for different growth directions. This is pronounced in crystals, grown from solutions and supercooled melts, which develop planar growth (habit) faces and, thus, consist of regions (*growth sectors*) grown in discrete directions defined by the normals of the growth faces involved (Fig. 4.8b). Among all habit faces that are possible in principle, the *final* crystal usually exhibits only those faces which possess low surface (attachment) energies and thus – according to Wulff's theorem [4.19–21] – have low growth velocities. *Fast* faces with higher attachment energy grow out and vanish from the external morphology (see *Wulff–Herring construction* [4.20–23]). Thus the crystal may contain more growth sectors, usually in close neighbourhood of the seed crystal, than are recognized from its final outward morphology (Fig. 4.8b).

Growth sectors are separated by growth-sector boundaries. These boundaries are internal surfaces over which the edges between neighboured faces have swept during growth. They are surfaces generated by the parallel movement of a straight line. When projected parallel to the edge (zone axis) of the two faces 1 and 2 involved, the boundary appears as a straight or somewhat curved line, the (local) direction of which depends on the (instantaneous) relative growth velocity v_1/v_2 of these faces (Sect. 4.3.6 and Fig. 4.14). If v_1/v_2 is constant, the line is straight (i. e., the boundary is planar), if v_1/v_2 fluctuates, the line is irregular, often zigzag-like as sketched in Fig. 4.8a (i. e., the boundary is an irregularly waved surface).

Growth-sector boundaries and their surroundings may be perfect crystal regions. In many cases, however, they are fault surfaces which can be observed by etching, optical birefringence and x-ray diffraction topography. The fault may be due to increased local impurity incorporation when growth layers on neighboured faces meet at their common edge, or to slightly different lattice parameters in both sectors. The latter lead to a transition zone along the boundary with lattice distortions which can be detected by the meth-

ods just mentioned. An example for this case is shown in Fig. 4.11. Lattice distortions preferentially occur along boundaries between symmetrically *nonequivalent* faces, due to different incorporation of impurities (see previous Sect. 4.2.1) which leads to slight differences of their *d*-values. Boundaries between symmetrically *equivalent* sectors are often strain-free, but may be visible by the sharp bends of growth striations (if present), see Fig. 4.9. An illustrative example of the extraordinarily rich growth sectoring of natural beryl, revealed by x-ray topographic imaging of sector boundaries and striations, is presented by *Herres* and *Lang* [4.52]. For the x-ray topographic characterisation of faulted growth-sector boundaries as shift or tilt boundaries, see *Klapper* [4.7, 8, 53].

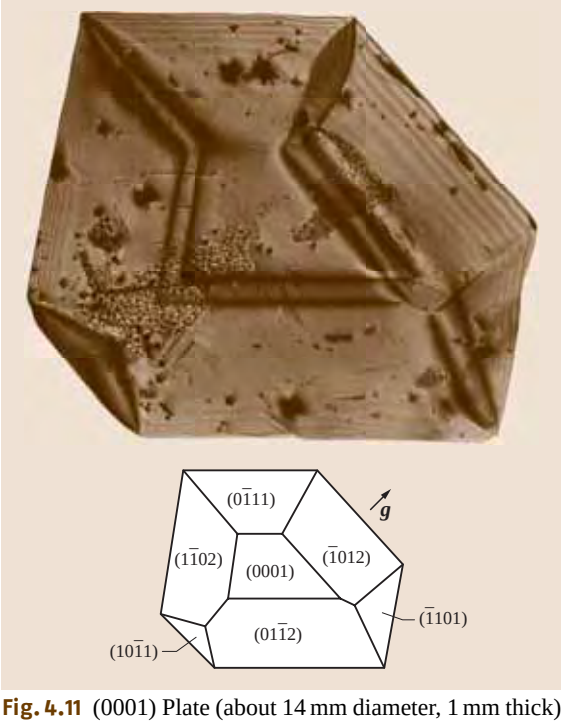

Fig. 4.11 (0001) Plate (about 14 mm diameter, 1 mm thick) of benzil grown from solution in xylene, containing faulted boundaries between the growth sectors shown in the drawing. The boundaries are inclined to the plate normal and appear as contrast bands with increased intensity at their emergence at the surface (increased strain due to stress relaxation at the surface). Some boundaries are invisible in the x-ray reflection used here. The plate tapers toward its edges, thus giving rise to *pendelloesung* fringes. Some contrasts are due to surface damages. Diffraction vector $\boldsymbol{g}(\bar{2}020)$, CuK$\alpha_1$ radiation

The different incorporation of additives in different growth sectors is strikingly demonstrated in the so-called *dyeing of crystals* which goes back to Sénarmont (1808–1862) and was in the last two decades extensively studied by *Kahr* and coworkers (e.g. [4.29, 30]). They grew crystals from solutions with organic dye molecules as additives. The distinct incorporation of these molecules on different growth faces is conspicuously apparent from the different colouring of their growth sectors (see also Sect. 4.3.5 *Optical Anomalies* below). A similar study of colouring the growth sectors of KDP with organic dyes is reported by *Maeda* et al. [4.54].

4.3.3 Vicinal Sectors

Another, less pronounced kind of sectoring frequently arises within the growth sectors, treated above, by growth hillocks (growth pyramids). These very flat *vicinal* pyramids, which are caused by dislocations emerging at their apex, often exhibit facets (*vicinal facets*) deviating by only very small angles from the main growth face. The facets are formed by terraces of growth layers, and their slopes depend on the step height and the widths of the terraces. On facets with different slope angles the incorporation of impurities is different. This leads to slightly distinct *d*-values of the regions grown on different vicinal facets (*vicinal sectors*). In analogy to growths sectors, the ridges of the vicinal pyramids form the *vicinal-sector boundaries*, which may be faulted surfaces. This also holds for the *valleys* between neighboured vicinal pyramids.

A detailed x-ray topographic study of vicinal sectors and their boundaries, formed on {101} dipyramid faces and {100} prism faces of KDP and ADP was published by *Smolsky* et al. [4.55] and *Smolsky* and *Zaitseva* [4.56], who also coined the term *vicinal sector*. An atomic-force microscope in-situ investigation of the step structures of vicinal hillocks in relation to the Burgers vectors of unit and multiple unit height of the dislocations generating the hillocks is presented by *De Yoreo* et al. [4.57]. Pronounced triangular vicinal pyramids are observed on {111} octahedron faces of potassium alum (cf. the optical and x-ray topographic study by *Shtukenberg* et al. [4.58], and *Klapper* et al. [4.59]). Tetragonal vicinal pyramids generating faulted sector boundaries on {001} faces of tetragonal nickel sulphate hexahydrate have been studied by *van Enckevort* and *Klapper* [4.60]. The impurity incorporation on different slopes of vicinal hillocks on {111}

boundary in the corresponding growth stage. Thus, the relative growth rates are easily reconstructed if the growth-sector boundary is visible.

An illustrative example, showing the strong changes of the growth velocities (*growth-rate dispersion*) due to fluctuations of growth conditions and defects is presented in Fig. 4.15a,b [4.59, 75]. It shows x-ray topographs of a (110) plate cut from a potassium alum crystal (grown from aqueous solution by temperature lowering) which was subjected to a temporary redissolution by a temporary temperature increase of about 1 °C [4.27]. The two boundaries between the central cube sector (001) and the two neighboured octahedron sectors ($\bar{1}11$) and ($1\bar{1}1$) are clearly depicted by kinematical contrast due to lattice distortions. (For the contrast variations in different x-ray reflections, see Chap. XX by *Dudley* in this Handbook.) Figure 4.15c outlines the shape of the crystal in different stages of growth, reconstructed from the course of the growth-sector boundaries (dotted line). Four regions (1)–(4) of different relative growth rates are distinguished. In the first period, after seeding-in, the crystal was grown by continuous temperature decrease of about 0.3 °C/day until it reached the shape outlined by A-A-A-A. At this stage the temperature of the growth chamber was increased in one step by 1 °C. Due to the slow transfer of the temperature jump into the solution, redissolutions started about half an hour later, recognized by the rounding of the crystal edges. Now the previous temperature and decrease rate was restored and growth continued as before. By this disturbance a layer of liquid inclusions covering a part of the (001) facet was formed, and its growth rate, relative to the neighboured {111} faces (the growth rate of which remained constant during the whole experiment), was strongly increased in region (2). In regions (3) and (4) it decreased again. From the angles β_1, β_2 ($\alpha = 35.26°$) the relative growth rates were determined to

$$v(001)/v(111) = 1.0/5.6/1.7/0.8$$

in growth intervals (1)/(2)/(3)/(4)

(averaged over the nearly equal left and right-hand sides). The drastic increase in period (2) is obviously due to the dislocations originating from the inclusions,

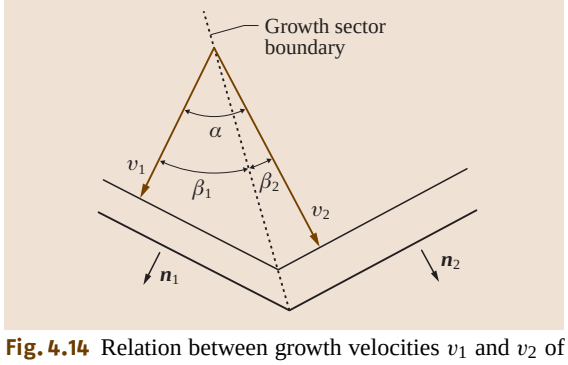

Fig. 4.14 Relation between growth velocities v_1 and v_2 of neighboured growth faces (growth direction $\boldsymbol{n}_1$ and $\boldsymbol{n}_2$) and the direction of the growth-sector boundary (*dotted line*)

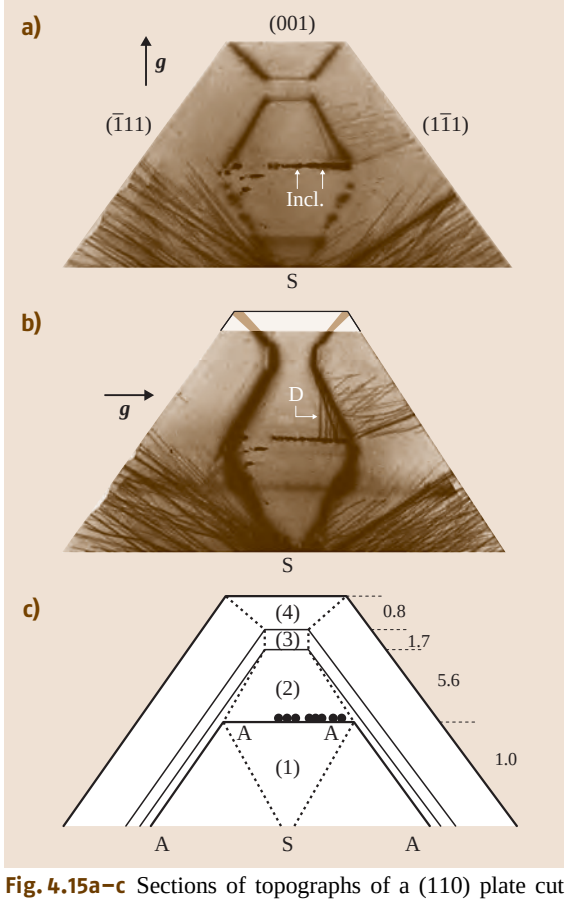

Fig. 4.15a–c Sections of topographs of a (110) plate cut from a potassium alum crystal subjected to a temporary redissolution (vertical extent 12 mm, reflections 004 **(a)** and 220 **(b)**). S: location of the seed (outside the section); Incl.: liquid inclusion; D: edge dislocations. **(c)** Illustration of the development of the crystal shape and of growth-sector boundaries (*dotted lines*) during growth. Contours A-A-A-A outlines the shape of the crystal at the time of redissolution. At the right side the relative growth rates $v(001)/v(111)$ of growth intervals (1) to (4) are given (after [4.75])

and the retardation in periods (3) and (4) may arise from the elimination of these dislocation from the (001) face by bending at the growth-sector boundary into the (111) sector. Note that only a part of the dislocations involved in this process is visible in the topographs (Fig. 4.15a,b) of the 1.4 mm thick crystal cut, since the larger part of the (001) sector (with a basis of about $8 \times 8\,\mathrm{mm}^2$ in growth stage A-A-A-A) is outside the cut and thus not recorded. In this context reference is made to similar and more detailed studies on the dislocation-dependent growth rate dispersion of {100} and {110} growth faces of potassium alum by *Sherwood* and *Shiripathi* [4.76], *Bhat* et al. [4.77] and *Ristic* et al. [4.78]. An interesting output of their investigations is the evidence of the growth-promoting role of pure edge dislocations (Sect. 4.4.7).

4.4 Dislocations

4.4.1 Growth Dislocations and Post-Growth Dislocations

Dislocations are generated during crystal growth, by plastic deformation and by the condensation of self-interstitials and vacancies. In the study of crystal growth defects it is useful to distinguish between two categories of dislocations:

1. Dislocations, which are connected with the growth front and proceed with it during growth (*growth dislocations* or *grown-in dislocations*); and
2. Dislocations, which are generated *behind* the growth front, either still during the growth run or during cooling to room temperature (*post-growth dislocations*), or later during processing or by improper handling

The final arrangement of dislocations in a crystal at room temperature results from growth dislocations, post-growth dislocations and the movement, multiplication and reactions of both after growth. Crystals grown at low temperatures (e.g., from aqueous solution) and in their brittle state usually contain dislocations in their original *as-grown* configuration; whereas in crystals grown at high temperatures, the original dislocation configurations may be drastically altered by dislocation movement, dislocation multiplication and dislocation reactions. These processes, which may occur during the growth run (*behind* the growth front), are induced by thermal stress due to temperature gradients and, particularly in crystals grown at very high temperatures, by the absorption of interstitials and vacancies (*dislocation climb*).

In this chapter the formation and propagation of dislocations in crystals grown at low temperatures (below 100 °C) under zero or only low thermal gradients are treated. The development of dislocation configurations during growth from melt under high thermal gradients or during processing at elevated temperatures has been experimentally and theoretically studied by various authors (e.g. [4.79–82]) and is reviewed by *Rudolph* in Chap. XX of this Handbook.

4.4.2 Sources of Growth Dislocations

For topological reasons dislocations lines cannot start or end in the interior of a perfect crystal. They either form closed loops, or they start from external and internal surfaces (e.g., grain boundaries), or from other defects with a *break* of the crystal lattice. In crystal growth, such defects may arise from all kinds of inclusions (e.g., foreign particles, liquid inclusions, bubbles, solute precipitates). When inclusions are overgrown and *closed* by growth layers, *lattice closure errors* may occur. These errors are the origin of growth dislocations which are connected to the growth front and propagate with it during further growth.

It is a very common observation that inclusions are the source of growth dislocations. Examples are shown in Figs. 4.3, 4.5, 4.10, etc. The appearance of dislocations *behind* an inclusion (viewed in the direction of growth) is correlated with its size: small inclusions emit only a few dislocations or are often dislocation-free. Large inclusions ($> 50\,\mu\mathrm{m}$) usually emit bundles of dislocations. In some cases, however, large inclusions (several millimeters in diameter) of mother solutions *without* dislocation generation have been observed (e.g., in the capping zone of KDP [4.83, 84]).

The generation of growth dislocations by foreign-particle inclusions has been experimentally studied by *Neuroth* [4.85] on crystals growing in aqueous solution (potassium alum) and in supercooled melt (benzophenone $(C_6H_5)_2CO$, $T_m = 48\,^\circ\mathrm{C}$; salol $C_{13}H_{10}O_3$, $T_m = 42\,^\circ\mathrm{C}$). A seed crystal is fixed to a support in such orientation that a dominant growth face (octa-

hedron (111) for cubic potassium alum, prism (110) for orthorhombic benzophenone, pinacoid (100) for orthorhombic salol) develops horizontally. After a sufficiently long distance of (visually) perfect growth, a small ball of solder (0.3–0.5 mm) is placed on the horizontal growth face, and growth continued without change of conditions. During the whole experiment the growth surface was observed with a microscope (long focal distance) in reflected light or by Michelson interferometry, both with video tape recording. After the deposition of the ball the face grows slowly as before without additional surface features as long as the ball is not covered by growth layers. During this period the crystal seems to *sink* into the growing crystal. In the moment when the ball is covered by growth layers, a sudden hectic criss-cross movement of growth steps is observed, which after some ten minutes *calms down* and develops into several slowly growing spiral hillocks. During further growth the number of hillocks is reduced to a few dominating growth hills which have *overrun* other hills.

For the study of the dislocations associated with the inclusions, a plate containing the ball and the region *behind* it was cut out of the crystal and subjected to x-ray topography. Figure 4.16 shows that numerous dislocations, propagating with the growth front, originate from the *back side* of the ball. Their density is partially too high to be resolved by this imaging method.

Similar experiments have been performed with mechanical in-situ violation (puncturing, scratching) of an interface perfectly and steadily growing in solution, supercooled melt and by Czochralski pulling [4.85]. Again, bundles of dislocations originate from these damages, which in solution growth usually give rise to liquid inclusions. In plastic crystals (always the case in melt growth) the mechanical impact generates glide dislocations which emerge at the growth front and continue as growth dislocations. Similar experiments are reported by *Forty* ([4.86, esp. p. 23]). His review presents a rich collection of photographs of growth spirals and other surface patterns on growth faces of various crystals.

The formation of screw dislocations in thin plates of organic crystals during growth from solution and from the vapour has been studied in-situ by Russian authors using (polarised) light microscopy with film recording [4.87–89]. Screw dislocations arise at reentrant corners between branches of dendrites [4.87] and by growth around intentionally introduced particles [4.88, 89]. In these cases the dislocations run through the lamellae and do not end inside the crystal. The mechanism of the formation of lattice closure errors and of dislocations *behind* an inclusion on nanometer scale is not yet fully understood although simple models have been derived. An example is presented by *Dudley* et al. [4.90].

As has been pointed out (*Fluctuation of Growth Conditions (Growth Accidents)*)para]Paragraphs have no number. So they can't be referenced by bumber. Please confirm this change., in habit-face crystals inclusions preferentially arise in the regeneration zone of growth on rounded interfaces, in particular in the zone of first growth on a seed crystal. Moreover, dislocations and other defects (grain boundaries, twins) pre-existing in the seed will continue into the growing crystal. Thus, the perfection of the seed as well as the seeding-in process are most crucial for the growth of perfect crystals. This holds for all methods of seeded growth, not only for habit-face crystals. That the regeneration zone around the seed crystal is the main source of dislocations is apparent from several topographs shown in this review. It is stressed that inclusions and dislocations can largely avoided by very slow (and thus time-consuming)

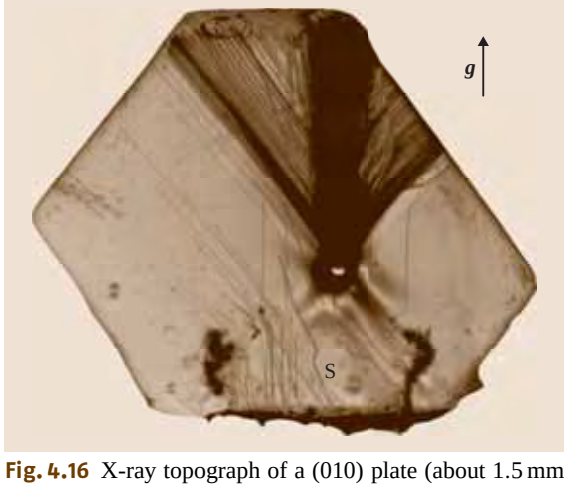

Fig. 4.16 X-ray topograph of a (010) plate (about 1.5 mm thick, width 21 mm) cut from a crystal of orthorhombic salol grown in supercooled melt. It contains a solder ball (diameter about 0.4 mm) dropped on a perfectly growing (100) facet (directed upward). Numerous dislocations were generated *behind* the ball. Dislocations of the fan propagating to the left are pure screw and exactly parallel to one of the prominent ⟨101⟩ edges which dominate the shape of the crystal (cf. *Deviations from Calculated Directions* (i) and Fig. 4.22). The (not resolved) dislocations of the vertical bundle have Burgers vectors [100] and [001]. Diffraction vector $\boldsymbol{g}(200)$, CuKα_1

growth during the regeneration period of first growth on a perfect seed.

Finally it is emphasized that inclusions can also block already existing dislocations. This has several times been observed by the author and reported in the literature. It frequently happens to dislocations in the seed crystal which are blocked by inclusions formed in the regeneration zone (*capping*) of first growth and do not enter the growing crystal [4.83,84]. Thus provoking a capping zone by an intentionally introduced deviation of the seed surface from a habit face may be helpful for reducing the number of dislocations coming from the seed, but it implies also a considerable risk of generating *new* dislocations behind the inclusions. The blocking of growth dislocations by closed inclusions must obey the conservation law of Burgers vectors as discussed in the following Sect. 4.4.3.

4.4.3 Burgers Vectors, Dislocation Dipoles

The sum of the Burgers vectors of all dislocations originating from a closed inclusion embedded in an otherwise perfect crystal is zero [4.83]. This directly follows from Frank's conservation law of Burgers vectors (see text books on dislocations, e.g. [4.91–93]) which states that the sum of Burgers vectors $\boldsymbol{b}_i$ of all dislocation lines going into a dislocation node (i. e., with line direction *into* the node) is zero $\sum \boldsymbol{b}_i = 0$ (analogous to Kirchhoff's law of electrical currents). Another proof may be given via the Burgers-circuit definition of Burgers vectors (e.g. [4.91–93]): imagine a Burgers circuit parallel the growth face in the perfect crystal region grown before the inclusion was formed. Now shift the circuit stepwise in growth direction over the inclusion and the dislocation bundle behind it. No closure error of the circuit, which now encircles all dislocations, will arise during this (virtual) procedure: $\sum \boldsymbol{b}_i = 0$.

From this it immediately follows that a *single* dislocation cannot originate from an inclusion. If dislocations are formed, there must be at least two of them, with opposite Burgers vectors. This is often observed when the inclusions are very small. Two slightly diverging dislocation lines emanating from small, x-ray topographically invisible or nearly invisible inclusions were observed in KDP by *Fishman* [4.83]. Examples are presented in Fig. 4.19 (label A) for salol grown from supercooled melt. A few pairs of slightly diverging dislocations, starting from a point, can also be recognized in Fig. 4.10 of a Czochralski salol specimen. There are, however, many x-ray topographic observations of only one dislocation line arising from an inclusion (e.g., in Fig. 4.3, where only one stronger contrast line comprises the image of more than one dislocation). In these cases the line must represent a pair of two closely neighboured (x-ray topographically not resolved) parallel dislocations with opposite Burgers vectors: a dislocation dipole. Such a dipole can alternatively also be considered as a single dislocation in the shape of a narrow hairpin with its (virtual) bend in the inclusion. In this approach the two branches of the *hairpin* have the same Burgers vector, but opposite directional sense. Examples of a pure-screw and two pure-edge dislocation dipoles are shown in Fig. 4.17. The two branches of the dipoles attract each other and may annihilate if they come close enough together. This annihilation is possible for screw dislocation dipoles, and for edge dipoles if both edge dislocations of the latter are on the same glide plane. If they are located on different glide planes,

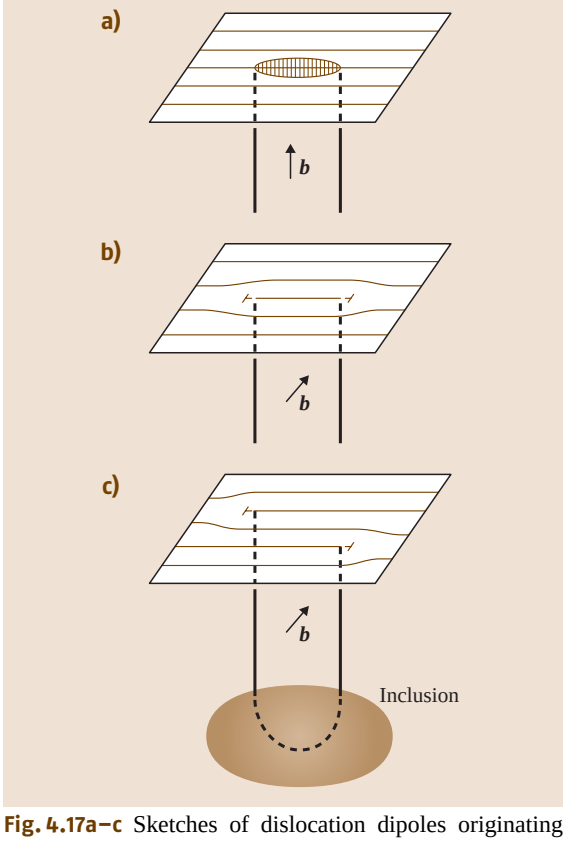

Fig. 4.17a–c Sketches of dislocation dipoles originating from an inclusion. Here the dipoles are considered a single (hairpin) dislocation with Burgers vector ***b*** but opposite line direction sense of the two branches. **(a)** Pure-screw dipole; **(b)** and **(c)**: Pure-edge dipoles

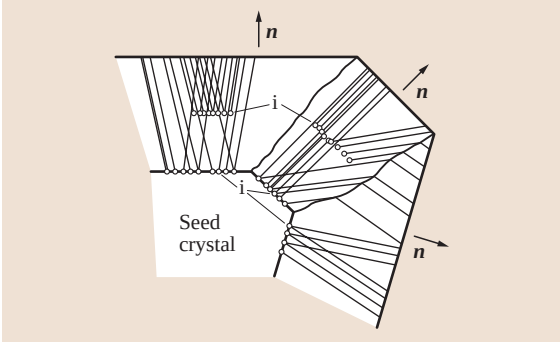

Fig. 4.18 Typical geometry of growth dislocations in crystals grown on habit faces. The different preferred directions of dislocations lines within one growth sector result from different Burgers vectors. These directions abruptly change their directions when they penetrate a growth-sector boundary, i. e., when, during growth, their outcrops shift over the edge from one face to the other (i: Inclusions)

the two dislocations can approach each other to a minimum separation, where they have prismatic character and form the edges of stripes of inserted or missing lattice planes (Fig. 4.17b). A model of the formation of a screw dislocation *behind* an inclusion is presented by *Dudley* et al. [4.90].

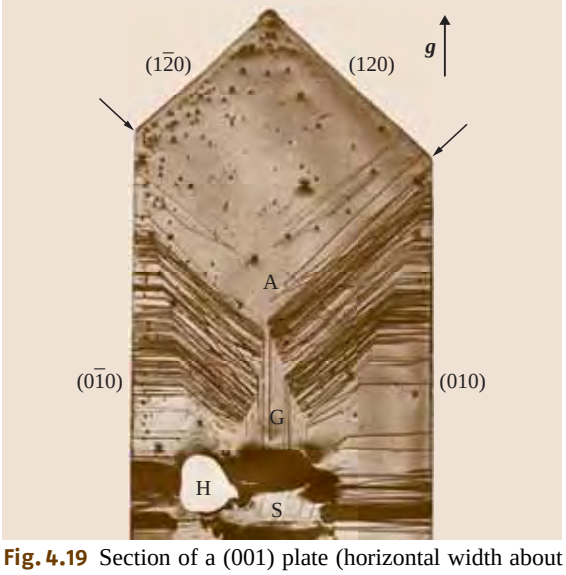

Fig. 4.19 Section of a (001) plate (horizontal width about 26 mm, thickness 1.5 mm) cut out of a salol crystal grown from supercooled melt. The dislocation lines change their preferred directions when they penetrate the boundaries (*arrows*) from the (120) sector into the {010} growth sectors. A: Dislocation pairs originating from tiny inclusions. Dots: surface damages. Diffraction vector $\boldsymbol{g}(200)$, CuKα

During x-ray topographic studies of growth dislocations it is often observed that *only one* contrast line originates from an inclusion, indicating – at first sight – a single dislocation (Fig. 4.3). Here the question arises, how by x-ray topography a dislocation dipole can be distinguished from a single dislocation with the same Burgers vector. If the dipole dislocations are sufficiently separated, they are resolved as two lines or appear as a broader contrast line. However, since the strain fields of the two dislocation have opposite signs and subtract each other, the resultant strain may also be smaller and less extended, if the separation of the two dislocations is small. Thus a dipole may appear on x-ray topographs by similar of even narrower contrast than a single dislocation with the same Burgers vector, and a distinction of both is often not immediately possible. An example is shown in Fig. 11a of *van Enckevort* and *Klapper* [4.60], where a single contrast line represents a screw dislocation dipole in nickel sulphate hexahydrate, as is proven by the bulge of one of the two dipole arms. In the same crystal the presence of two closely neighboured etch pits at the apices of growth pyramids and slip traces indicating the escape of one of the two screw dislocations from the hillock center have been observed. Dislocation dipoles are also formed during plastic flow of crystals, when the movement of glide dislocations is locally blocked by obstacles (inclusions, jogs). Examples are given in Sect. 4.4.5 (Figs. 4.25, 4.26).

4.4.4 Propagation of Growth Dislocations

Characteristic Configurations, Theory of Preferred Direction

A dislocation line ending on a growth face will proceed with this face [4.7, 8, 94]. Its direction depends on the shape and the orientation of the growth face and on its Burgers vector. As was shown in Sect. 4.3.2 and Fig. 4.8b, crystal growing on planar (habit) faces consist of growth sectors belonging to different growth faces (different growth directions $\boldsymbol{n}$). This leads – under ideal conditions (i. e., stress-free growth) – to a characteristic configuration of growth dislocations which is illustrated in Fig. 4.18. The dislocations start from inclusions and propagate as straight lines with directions $\boldsymbol{l}$ usually close to, and frequently parallel to, the growth direction of the sector in which they lie. They usually exhibit sharply defined, often noncrystallographic *preferred directions* $\boldsymbol{l}_0$ which depend on the growth direction $\boldsymbol{n}$ and on the Burgers vector $\boldsymbol{b}$: $\boldsymbol{l}_0 = \boldsymbol{l}_0(\boldsymbol{n}, \boldsymbol{b})$. The dependence

of the preferred direction $\boldsymbol{l}_0$ on the growth direction $\boldsymbol{n}$ becomes strikingly apparent when the dislocations penetrate growth-sector boundaries. This implies an abrupt change of the growth direction: the dislocation lines undergo an abrupt change of their preferred direction $\boldsymbol{l}_0$. An example is shown in Fig. 4.19.

These preferred direction of growth dislocations are explained by two approaches [4.7, 8, 94]:

1. *Minimum-energy theorem* (Fig. 4.20a). The dislocation lines adopt a direction $\boldsymbol{l}$ (unit vector), for which its energy within any growth layer is a minimum. For a growth layer of unit thickness $d = 1$ this can be expressed as

$$E/\cos\alpha = \text{minimum}\,,$$

with $E = E(\boldsymbol{l}, \boldsymbol{b}, c_{ij})$ the elastic energy (strain energy) per unit length of the dislocation line (c_{ij} are the elastic constants of the crystal) and α the angle between $\boldsymbol{n}$ and $\boldsymbol{l}$. The factor $1/\cos\alpha$ accounts for the length of the dislocation line in the layer.

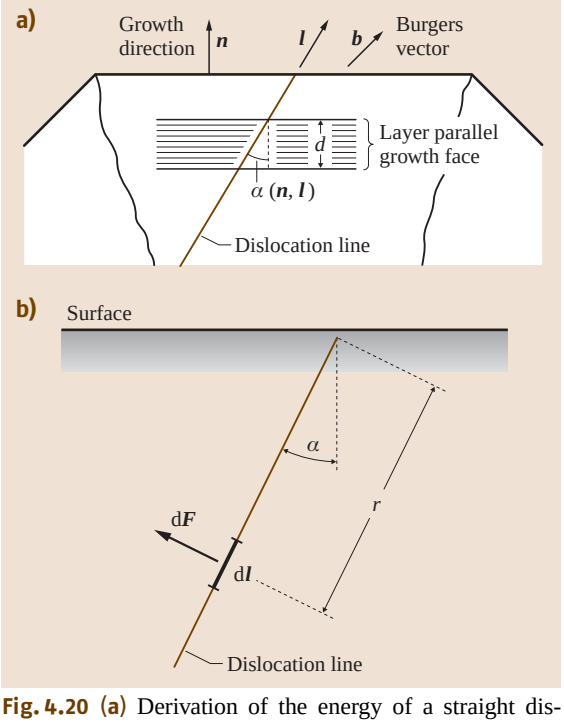

Fig. 4.20 (a) Derivation of the energy of a straight dislocation line within a layer parallel to the growth face. (b) Illustration of the force $\mathrm{d}\boldsymbol{F}$ exerted by the crystal surface upon a line segment $\mathrm{d}\boldsymbol{l}$ of a straight dislocation line emerging at the surface (theorem of *Lothe* [4.95])

2. *Zero-force theorem* (Fig. 4.20b). A dislocation line emerging at the surface experiences a force $\mathrm{d}\boldsymbol{F}$ which depends on the angle α between the dislocation direction $\boldsymbol{l}$ and the surface normal $\boldsymbol{n}$. At the surface this force is infinitely large. According to *Lothe* [4.95] there exists always a direction $\boldsymbol{l}_0$ for which this force is zero for the dislocation line segments at any depth below the surface. It is plausible that a dislocation emerging at the growth face follows during growth this direction of zero force.

Using the formula

$$\mathrm{d}F = -\frac{1}{r}\left(\frac{\partial E}{\partial \alpha} + E\tan\alpha\right)\mathrm{d}\boldsymbol{l}$$

(theorem of *Lothe* [4.95]), it can be shown that both approaches lead to the same preferred directions.

Verification of the Minimum-Energy Approach

The strain energy [4.7, 8, 94] per unit length of a straight dislocation line is given by (see textbooks on dislocations, e.g. [4.91–93])

$$E = \frac{Kb^2}{4\pi}\ln\left(\frac{R}{r_0}\right)\,,$$

with $K = K(\boldsymbol{l}, \boldsymbol{l}_\mathrm{b}, c_{ij})$ the so-called energy factor of a straight dislocation line, R the outer cut-off radius and r_0 the inner cut-off radius, and b the modulus of the Burgers vector $\boldsymbol{b}$. The energy factor K describes the variation of the strain energy with the direction $\boldsymbol{l}$ of the dislocation line. It also depends on the on the Burgers vector direction $\boldsymbol{l}_\mathrm{b}$ and on the elastic constants c_{ij} of the crystal. The inner cut-off radius defines the limit until which the linear elasticity theory is applicable, and it corresponds to the radius of the dislocation core.

Since the logarithmic term and the core energy are, in general, not accessible to a numerical calculation, the variation of strain energy E of a given dislocation with Burgers vector $\boldsymbol{b}$ with direction $\boldsymbol{l}$ is – in a certain approximation – considered as proportional to the energy factor $K(\boldsymbol{l}, \boldsymbol{l}_\mathrm{b}, c_{ij})$, assuming the logarithmic term as independent of $\boldsymbol{l}$. The energy factor has been calculated using the theory of dislocations in elastically anisotropic crystals developed by *Eshelby* et al. [4.96]. Since, in general, analytic solutions are not possible, numerical calculations have been performed using a program DISLOC, accounting for elastic anisotropy of any symmetry down to the triclinic case [4.94]. Figures 4.21a,b show the comparison of observed and calculated preferred directions of dislocations with four different Burgers vectors in the (101)

growth sector of KDP [4.97]. The agreement is excellent with deviations of 3–6°, except for dislocation 4, the observed directions of which scatter by ±5° around a direction deviating by about 20° from the calculated one. This may be due to the very flat minimum of K, which makes the minimum energy directions more subject to other influences like surface features and core-energy variations (see *Deviations from Calculated Directions*). Similar comparisons have been carried out for various crystals grown on planar faces from solutions and supercooled melts (benzil, $(C_6H_5CO)_2$ [4.53, 98]); thiourea, $(NH_2)_2CS$ [4.99], lithium formate monohydrate $HCOOLi \cdot H_2O$ [4.100], ammonium hydrogen oxalate hemihydrate, $NH_4HC_2O_4 \cdot 1/2H_2O$ [4.101], zinc oxide, ZnO [4.94]. In general, the agreement of observed and calculated directions is satisfactory and confirms the validity of the above theorems. It is pointed out that the preferred directions are independent of the growth method, provided that the growth faces (growth sectors) are the same. This has been demonstrated for benzil grown *in solution* in xylene and *in supercooled melt* ([4.1], [4.7, p. 138 and Fig. 17 therein]). Moreover, basal growth dislocations (Burgers vectors $\boldsymbol{b} = \langle 100 \rangle$) in prism sectors of hydrothermally grown hexagonal (wurtzite-type) ZnO crystals [4.102] show the same minimum-energy configuration as the corresponding growth dislocations in the prism sectors of benzil [4.94]. This similarity is due to the hexagonal lattice, the same prism growth sector and the same Burgers vectors of the dislocation in both cases.

An interesting experimental study of preferred dislocation directions in synthetic quartz is presented by *Alter* and *Voigt* [4.103]. They have cut (0001) plates (Z-plates) out of different growth sectors of previously grown highly perfect quartz crystals and used them as seed plates for further growth experiments. The seed plates contained growth dislocations following the preferred directions typical for the sector from which they were cut. Since growth now proceeded on the (0001) face, the dislocations of the seed continued into the growing crystals with preferred directions typical for the Z-sector, exhibiting sharp bends of up to 90° at their transition from the seed into the grown crystal. This is instructively shown by x-ray topography [4.103].

On account of the factor $1/\cos\alpha$ in the energy term above, the preferred directions of growth dislocations

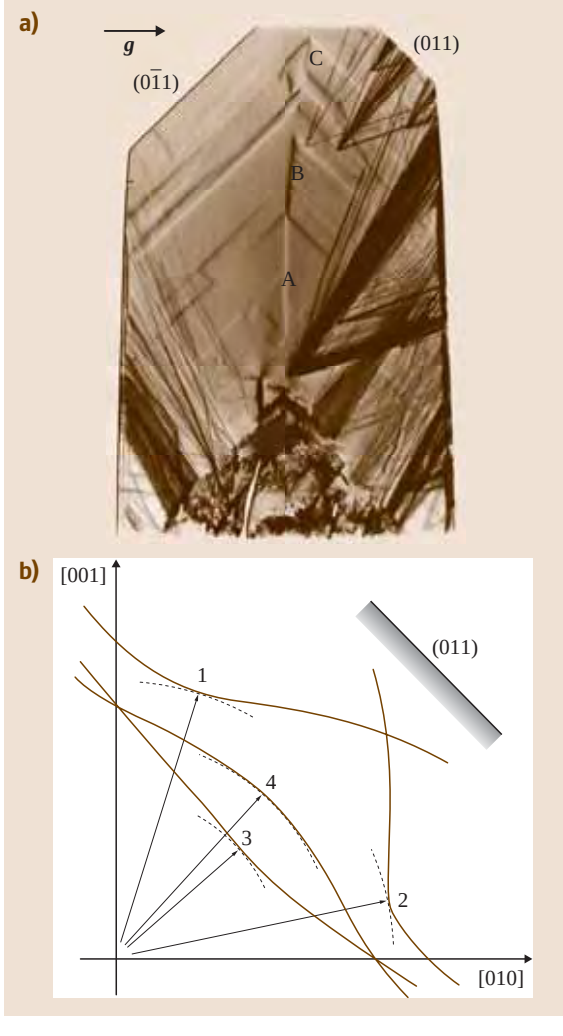

Fig. 4.21 (a) X-ray topograph ($\boldsymbol{g}$(020), Ag-Kα radiation) of a KDP (100) plate (horizontal width ≈ 28 mm, thickness ≈ 1.5 mm), showing bundles of dislocations with non-crystallographic preferred directions emanating from small liquid inclusions (especially in the right-hand (011) growth sector) and from the capping region. The Burgers vectors of these dislocations can be recognized form their preferred directions. In addition, growth bands and features due o vicinal effects are visible. ABC: Boundary between (011) and (0$\bar{1}$1) growth sectors. (b) Plots of calculated energies $E/\cos\alpha$ (arbitrary units) of dislocations with Burgers vectors $\boldsymbol{b} = [001]$ (1), $\boldsymbol{b} = [100]$ (2), $\boldsymbol{b} = [011]$ (3) and $\boldsymbol{b} = [0\bar{1}1]$ (4) in growth sector (011) of KDP (polar coordinates: the energies are given by the length of the radius vector to the curves). The preferred directions of minimum $E/\cos\alpha$ are represented by *arrows*. The *dashed lines* are circles with radii equal to the minimum values of $E/\cos\alpha$. Note the close coincidence to observed (a) and calculated (b) dislocation line directions◀

are mostly normal or nearly normal to the (local) growth face. In some cases of planar interfaces, however, deviations from the growth normal of up to 30° have been observed in agreement with the calculations. For interfaces with convex curvature (e.g., in Czochralski growth) the dislocation lines diverge and grow out of the crystal boule through its side faces, whereas for concave interfaces the dislocation lines are focussed into the center of the crystal boule (Fig. 4.10). Trajectories of growth dislocations in Czochralski gadolinium gallium garnet (GGG) have been calculated and compared with observed ones by *Schmidt* and *Weiss* [4.68]. The curvature of the interface has been taken into account by performing the calculations stepwise in small increments, leading to curved dislocation trajectories. Again the agreement is satisfactory. Moreover, it allowed assigning Burgers vectors to the different dislocation trajectories which were observed optically in polarised light.

In 1997 and following years, preferred dislocations directions and their bending when penetrating a growth sector boundary have been observed by transmission electron microscopy in GaN grown by MOVPE (metal-organic vapour phase epitaxy) using the ELO (epitaxial lateral overgrowth) technique [4.105–109]. The GaN hexagonal pyramids $\{11\bar{2}2\}$ growing through the windows in the mask are in the first stage topped by the (0001) basal plane, which during further growth becomes smaller and finally vanishes. Thus growth dislocations propagating normal to the (0001) facet penetrate the boundary to a $\{11\bar{2}2\}$ sector and are bent by about 90° into the preferred direction in this sector [4.108]. Very recently the bending of dislocations in growth-sector boundaries has also been used for the elimination of threading dislocations by *aspect ratio trapping* in Ge selectively grown in submicron trenches on Si substrates [4.110]. Similarly, dislocations are eliminated from prism growth sectors of rapidly grown KDP crystals ([4.111, cf. Fig. 4 therein]).

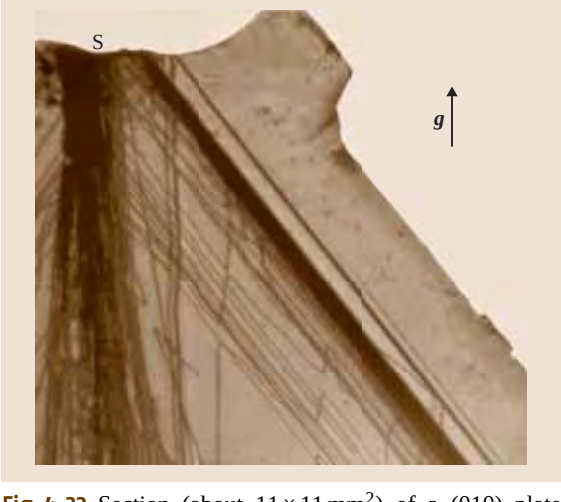

Fig. 4.22 Section (about $11 \times 11\,\mathrm{mm}^2$) of a (010) plate (about 1.3 mm thick) cut out of the cone region of a Czochralski salol (pulling direction [100] upward; S: seed crystal, broken off). The topograph shows many straight dislocation lines ($\boldsymbol{b} = [101]$) exactly parallel to ⟨101⟩ which is the most prominent morphological edge of the crystal (Fig. 4.16). This direction is enforced by the discrete lattice structure, because the minimum-energy continuum approach suggests directions close to the normal to the concave interface. Furthermore, reactions (segment-wise annihilation) with a few *vertical* dislocations are recognized ([4.104]). Diffraction vector $\boldsymbol{g}(200)$, CuKα_1

The above theory of preferred dislocation directions does not allow a dislocation line to proceed along a growth-sector boundary, as is sometimes discussed: the line would emerge on the edge constituting the boundary and thus be in a labile position. If, however, the edge is a narrow facet, the dislocation line can lie in its sector and appear to proceed along the boundary, but the probability of *breaking out* into one of the adjacent sectors would be high. *Ester* and *Halfpenny* [4.112] and *Ester* et al. [4.113] have observed in potassium hydrogen phthalate V-shaped pairs of dislocations originating from growth-sector boundaries, with the two *arms* of the *V*, following sharply defined directions, in the two adjacent sectors. This is in accordance with the minimum-energy concept.

Deviations from Calculated Directions

Although the agreement of observed and calculated directions of growth dislocations is in general satisfactory, frequently discrepancies are found. The reasons for this may be due to the insufficient approximation by the model on which the calculations are based, or by influences of other defects, or by a particular surface relief. The above calculations are based on linear anisotropic elasticity of the continuum and do not account for the discrete structure of the crystals, the dislocation core energy and, in piezoelectric crystals, for electrical contributions.

The following three causes have been found to affect preferred directions:

i. Discrete lattice structure of the crystals and the neglect of the core energy

benzophenone crystal (temperature of the melt about 1.5 °C above $T_m = 48$ °C, pulling rate 20 mm/day). During pulling the crystal was cooled by blowing air of about 35 °C against the rotating crystal in order to obtain a crystal diameter of 25 mm [4.43]. The topograph shows growth dislocations which originate from the zone of first growth on the seed crystal (outside the top of the figure). A few of the dislocations have still their original course (straight or slightly curved lines), but most of them have suffered post-growth movement (which may have occurred already during the pulling process): they consist of a series of bow-shaped segments connected at pinning points (right-hand side of Fig. 4.26). The pinning points are aligned along straight lines marking the original position of the dislocations. On the left-hand side of the Fig. Fig. 4.26 the changes are even more drastic: some dislocations have partially annihilated, leaving back only a few large and several small dislocation loops. Post-growth reactions of growth dislocations forming dislocation nodes in

Fig. 4.25 Section (about $4 \times 7\,mm^2$) of a (110) plate (about 1.5 mm thick) of benzophenone grown from supercooled melt. The *large arrows* mark four growth dislocation in a (111) sector showing sharply defined non-crystallographic preferred directions (predominantly screw character) in their upper, and post-growth movement with pinning stops in their lower parts. Burgers vector $\boldsymbol{b} = [001]$ vertical. The horizontal segments are pure-edge and form a few dislocation dipoles (*small arrows*). The dislocations emerge through the plate surfaces. $\boldsymbol{g}(002)$, CuKα_1

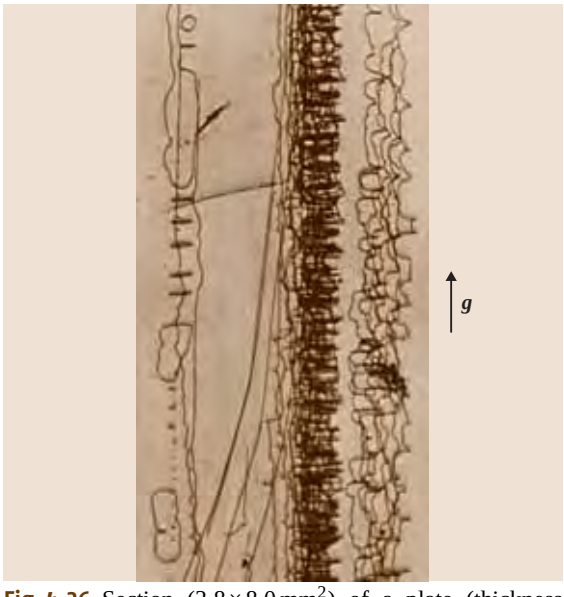

Fig. 4.26 Section ($3.8 \times 8.0\,mm^2$) of a plate (thickness about 1.2 mm) cut from a Czochralski crystal (pulling direction upward) of benzophenone ($T_m = 48$ °C), showing growth dislocation after post-growth movement. The pinning points of one of the dislocations at the right-hand side mark its originally straight course. At the left side some dislocations have partially annihilated and form closed loops. $\boldsymbol{g}(002)$, CuKα_1

Czochralski salol have been studied by *Neuroth* and *Klapper* [4.116].

Interestingly, the dislocations in Czochraski salol of Fig. 4.10 have preserved their growth configuration with straight lines roughly normal to the growth front, despite the thermal stress which is always present in this growth technique. This may be due to the low growth temperature ($T_m = 42$ °C) and the narrow plastic zone of salol below the melting point.

4.4.6 Post-Growth Dislocations

Dislocations formed in the interior of the already grown crystal without connection to the growth front or other surfaces must be closed loops [4.7–11]. It is practically impossible to generate closed loops in a perfect crystal by stress, since the stress required for such processes would be extremely high. Inclusions, however, usually represent stress centers and form internal surfaces in the crystal. The stress in the crystal around the inclusions is relieved by the emission of concentric dislocations loops or – more frequently – of disloca-

the x-ray topographs shown in Figs. 4.5, 4.21a, 4.23 and 4.33. The crystals shown in the former three figures have been grown in the 1970s in the laboratory of *Bennema* (Delft and Nijmegen, NL) in an three-vessel growth system [4.26] at constant temperature of about 30 °C and a supersaturation of about 5.4% with a growth rate about 1 mm/day on the {101} faces. The crystals were mounted on a tree which rotated in the solution. They contain inclusions, inhomogeneous impurity distributions (in the form of striations, growth and vicinal sectors) and dislocations. As was pointed out already by *Zerfoss* [4.12], *Janssen-van Rosmalen* et al. [4.26,32], *van Enckevort* et al. [4.33], liquid inclusions, in particular the quasi-periodic liquid inclusions in Fig. 4.5, can be avoided by strong stirring.

An x-ray topograph of an ADP crystal rapidly grown in the author's laboratory is shown in Fig. 4.33 [4.164]. The crystal was grown on a point seed in a sealed 10 l tank by temperature decrease from 55 to about 45 °C with about the same growth rates on {100} prism and {101} pyramid faces in ten days to a width of 110 mm along the ⟨100⟩ edges and a height of about 80 mm. It was rotated in the solution on a platform with about 50 cycles/min and reversal of the rotation every 30 seconds. The rate of temperature decrease was 0.1–1 °C in the generation period and is then stepwise increased to 4 °C/day, dependent on the size of the crystal. It is obvious from Fig. 4.33 that this crystal is much more homogeneous and perfect than the crystals shown in Figs. 4.5, 4.21a, 4.23. Only few dislocations originate from the point seed into the prism and pyramid growth sectors. Due to growth face instabilities large liquid inclusions have formed on the right prism face and but have perfectly healed out during further growth. Interestingly these inclusions block more growth dislocations than they generate. A convincing proof of the homogeneity of this crystal is the appearance of the x-ray *pendellösung fringes*, which result from the slight thickness decrease toward the edges of the plate. Neigh-

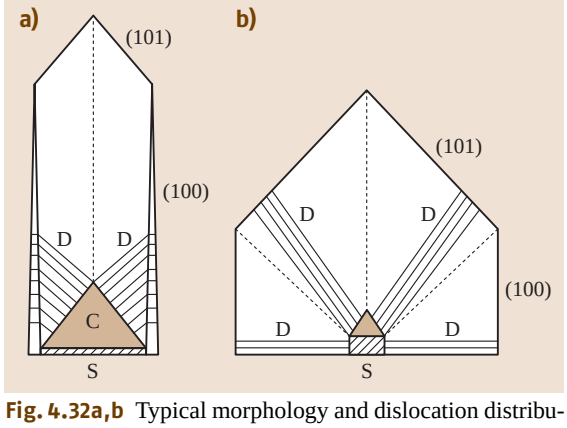

Fig. 4.32a,b Typical morphology and dislocation distribution of KDP and ADP crystal **(a)** slowly grown on a (001) seed plate S and **(b)** rapidly grown on a *point seed* S. D: Dislocation lines, C: strongly disturbed regeneration (*capping*) zone (Figs. 4.21, 4.23). In **(b)** this zone is small. *Dashed lines*: growth-sector boundaries

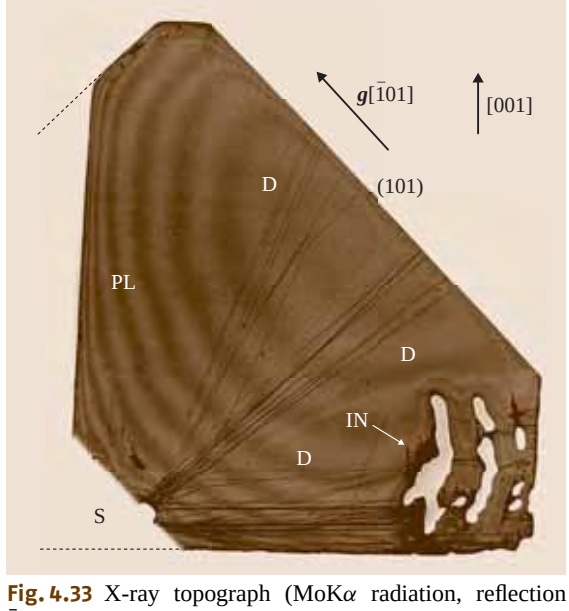

Fig. 4.33 X-ray topograph (MoKα radiation, reflection $\bar{1}01$) of a (010) plate (about 2.5 mm thick, horizontal extension about 60 mm, tetragonal axis vertical) cut from an ADP crystal rapidly grown within ten days (including the seeding-in process and regeneration period) to a size with ⟨100⟩ edge lengths of about 110 mm. S: Location of the seed. The crystal has grown with about the same growth rates (about 15 mm/day in the end phase) on all {100} and {101} faces. Since the plate was too big for the x-ray topography crystal holder, a part was cut off at the left side. The crystal is highly perfect, as indicated by the x-ray *pendellösung* fringes (rounded soft contrast bands) of constant plate thickness. Only few dislocations originate from a liquid inclusion at the point seed (which was out of the x-ray beam). IN: Large liquid inclusions which have formed on the right (100) face due to growth-face instabilities intentionally provoked by decreasing the temperature by 4 °C in one step at 50 °C after about 40 mm of perfect growth. Note that these inclusions have formed only on one of the four prism faces: the four {101} faces stayed also inclusion-free. Reflection $\boldsymbol{g}(\bar{1}01)$, MoK$\alpha$. After [4.164]

boured (010) crystal plates, not cutting though the seed and through the inclusions, are dislocation-free.

Rapid crystal growth of very large, highly perfect crystals from aqueous solution has been reported only for KDP, its deuterated variant DKDP and for ADP [4.36]. In order to check the applicability of this method to other materials, growth experiments have been carried out with some other compounds usually used in student laboratory courses: pure and mixed potassium and ammonium alums, sodium chlorate and nickel sulphate hexahydrate [4.164]. The growth procedure was essentially the same as reported above for ADP. Apart from some failures due to spontaneous nucleation, large crystals of these materials with edge lengths up to 12 cm could be successfully grown within 7–10 days with growth rates up to 25 mm/day. Optical inspection and x-ray topographic studies indicate that the optical and structural perfection is high and not at all inferior to the quality of corresponding traditionally grown crystals. These results indicate that the rapid-growth method is applicable to many crystals growing from solutions.

References

4.1 T. Scheffen-Lauenroth, H. Klapper, R.A. Becker: Growth and perfection of organic crystals from undercooled melt, J. Crystal Growth **55**, 557–570 (1981)

4.2 A.R. Lang: Techniques and interpretation in X-ray topography. In: *Diffraction and Imaging Techniques in Materials Science*, ed. by S. Amelinckx, R. Gevers, J. Van Landuyt (North-Holland, Amsterdam 1978) pp. 623–714, 2nd Edn.

4.3 A. Authier: X-ray and neutron topography of solution-grown crystals. In: *Crystal Growth and Materials (ECCG-1 Zürich)*, ed. by E. Kaldis, H.J. Scheel (North-Holland, Amsterdam 1976) pp. 516–548

4.4 B.K. Tanner: *X-ray Diffraction Topography* (Pergamon Press, Oxford 1976)

4.5 A.R. Lang: Topography. In: *Internat. Tables for Crystallography, International Union of Crystallography, Vol. C*, ed. by A.J.C. Wilson (Kluver Academic Publishers, Dordrecht 1995) pp. 113–123

4.6 H. Klapper: X-ray topography of twinned crystals. In: *Progress in Crystal Growth and Characterization*, Vol. 14, ed. by P. Krishna (Pergamon Press, Oxford 1987) pp. 367–401

4.7 H. Klapper: X-ray topography of organic crystals. In: *Crystals: Growth, Properties and Characterization*, Vol. 13, ed. by N. Karl (Springer, Berlin, Heidelberg 1991) pp. 109–162

4.8 H. Klapper: Defects in non-metal crystals. In: *Characterization of Crystal Growth Defects by X-ray Methods*, ed. by B.K. Tanner, D.K. Bowen (Plenum Press, New York 1980) pp. 133–160

4.9 H. Klapper: X-ray diffraction topography: Application to crystal growth and plastic deformation. In: *X-Ray and Neutron Dynamical Diffraction: Theory and Applications*, Proc. NATO ASI, Erice 1996, NATO Science Series B, Physics Vol. 357, ed. by A. Authier, S. Logomarsino, B.K. Tanner (Plenum Press, New York 1996) p. 167–177

4.10 H. Klapper: Structural defects and methods of their detection. In: *Materials Science Forum*, Vol. 276–277, ed. by R. Fornari, C. Paorici (Trans Tech Publications, Switzerland 1998) pp. 291–306

4.11 H. Klapper: Generation and propagation or dislocations during crystal growth, Mat. Chem. Phys. **66**, 101–109 (2000)

4.12 S. Zerfoss, S.I. Slawson: Origin of authigenic inclusions in synthetic crystals, Am. Mineralogist **41**, 598–607 (1956)

4.13 G. Laemmlein: Sekundäre Flüssigkeitseinschlüsse in Mineralien, Z. Kristallogr. **71**, 237–256 (1929), in German

4.14 A.R.J. de Kock: Effect of growth conditions on semiconductor crystal quality. In: *1976 Crystal Growth and Materials* (ECCG-1 Zürich), ed. by E. Kaldis and H.J. Scheel (North Holland, Amsterdam 1977) pp. 661–703

4.15 A.A. Chernov, D.E. Temkin: Capture of inclusions in crystal growth. In: *1976 Crystal Growth and Materials (ECCG-1 Zürich)*, ed. by E. Kaldis, H.J. Scheel (North Holland, Amsterdam 1977) pp. 4–77, esp. 53–54

4.16 V. Ya. Khaimov-Mal'kov: (a) The thermodynamics of crystallisation pressure; (b) Experimental measurement of crystallization pressure; (c) The growth conditions of crystals in contact with large obstacles. In: *Growth of Crystals*, Vol. 2, ed. A.V. Shubnikov, N.N. Sheftal (Consultants Bureau Inc., New York 1959) pp. 3–13 (a), 14–19 (b), 20–28 (c)

4.17 N. Zaitseva, J. Atherton, R. Rozsa, L. Carman, I. Smolsky, M. Runkel, R. Ryon, L. James: Design and benefits of continuous filtration in rapid growth of large KDP and DKDP crystals, J. Crystal Growth **197**, 911–920 (1999)

4.18 M.O. Kliia, I.G. Sokolova: The absorption of droplets of emulsion by a growing during crystallization from solutions, Sov. Phys. – Crystallogr. **3**, 217–221 (1958)

4.19 G. Wulff: Zur Frage der Geschwindigkeit des Wachstums und der Auflösung der Krystallflächen, Z. Kristallogr. **34**, 449–530 (1901), esp. 512–530, in German

4.20 R.F. Strickland-Constable: *Kinetics and Mechanisms of Crystallisation* (Academic Press, London, New York 1968) pp. 76–84

4.21 P. Bennema: Generalized Herring treatment of the equilibrium form. In: *Crystal growth: An introduction*, North-Holland Series in Crystal Growth I, ed. by P. Hartman (North-Holland, Amsterdam 1973), pp. 342–357

4.22 C. Herring: Some theorems on the free energies of crystal surfaces, Phys. Rev. **82**, 87–93 (1951)

4.23 C. Herring: The use of classical macroscopic concepts in surface energy problems. In: *Structure and Properties of Solid Surfaces*, ed. by R.G. Gromer, C.S. Smith (University of Chicago Press, Chicago 1953) pp. 5–72

4.24 W. Schnoor: Über das Wachstum von Auflösungskörpern und Kugeln aus Steinsalz, Z. Kristallogr. **68**, 1–14 (1928), in German

4.25 H.E. Buckley: *Crystal Growth* (Wiley, London, New York 1961)

4.26 R. Janssen-Van Rosmalen, W.H. van der Linden, E. Dobinga, D. Visser: The influence of the hydrodynamic environment on the growth and the formation of liquid inclusions in large potassium hydrogen phosphate crystals, Kristall und Technik **13**, 17–28 (1978)

4.27 A. Faber: *Röntgentopographische Untersuchungen von Wachstumsstörungen durch alternierende Temperaturgradienten im Kali-Alaun. Studienarbeit* (Inst. f. Kristallographie, RWTH Aachen 1980), in German

4.28 W.M. Vetter, H. Totsuka, M. Dudley, B. Kahr: The perfection and defect structures of organic hourglass inclusion K_2SO_4 crystals, J. Crystal Growth **241**, 498–506 (2002)

4.29 B. Kahr, R.W. Guerney: Dyeing crystals, Chem. Rev. **101**, 893–953 (2001)

4.30 B. Kahr, L. Vasquez: Painting crystals, Cryst. Eng. Comm. **4**, 514–516 (2002)

4.31 A.A. Chernov, G. Yu. Kuznetsov, I.L. Smol'skii, V.N. Rozhanski: Hydrodynamic effects during ADP growth from aqueous solutions in the kinetic regime, Sov. Phys. -Crystallogr. **31**, 705–709 (1986)

4.32 R. Janssen-Van Rosmalen, P. Bennema: The role of hydrodynamics and supersaturation in the formation of fluid inclusions in KDP, J. Crystal Growth **42**, 224–227 (1977)

4.33 W.J.P. van Enckevort, R. Janssen-van Rosmalen, H. Klapper, W.H. van der Linden: Growth phenomena of KDP crystals in relation to the internal structure, J. Crystal Growth **60**, 67–78 (1982)

4.34 N.P. Zaitseva, I.L. Smolsky, L.N. Rashkovich: Study of rapid growth of KDP crystals by temperature lowering, Sov. Phys. – Crystallogr. **36**, 113–115 (1991)

4.35 N.P. Zaitseva, J.J. De Yoreo, M.R. Dehaven, R.L. Vital, K.E. Montgomery, M. Richardson, L.J. Atherton: Rapid growth of large-scale (40 – 55 cm) KH_2PO_4 crystals, J. Crystal Growth **180**, 255–262 (1997)

4.36 N. Zaitseva, L. Carman: Rapid Growth of KDP-type Crystals, Progr. Crystal Growth Characteriz. Mater. **43**, 1–118 (2001)

4.37 I. Smolsky, J.J. de Yoreo, N.P. Zaitseva, J.D. Lee, T.A. Land, E.B. Rudneva: Oriented liquid inclusions in KDP crystals, J. Crystal Growth **169**, 741–745 (1996)

4.38 E. Scandale, A. Zarka: Sur l'origine des canaux dans les cristaux, J. Appl. Cryst. **15**, 417–422 (1982)

4.39 X.R. Huang, M. Dudley, W.M. Vetter, W. Huang, S. Wang, C.H. Carter Jr.: Direct evidence of micropipe-related pure superscrew dislocations in SiC, Appl. Phys. Lett. **74**, 353–355 (1999)

4.40 J. Heindl, H.P. Strunk, V.D. Heydemann, G. Pensl: Micropipes: Hollow tubes in silicon carbide, Phys. Stat. Sol. **162**, 251–262 (1997)

4.41 H.P. Strunk, W. Dorsch, J. Heindl: The nature of micropipes in 6H-SiC single crystals, Advan. Eng. Materials **2**, 386–389 (2000)

4.42 E. Roedder: Fluid inclusions. In: *Reviews in Mineralogy*, Vol. 12, ed. by P.H. Ribbe (Mineralogical Society of America, BookCrafters, Inc., Chelsea 1984)

4.43 Th. Scheffen-Lauenroth: *Czochralski-Züchtung und Perfektion organischer Kristalle*. Diplomarbeit (Inst. f. Kristallographie, RWTH Aachen 1983), in German

4.44 W. Bardsley, D.T.J. Hurle, M. Hart, A.R. Lang: Structural and chemical inhomogeneities in germanium single crystals grown under conditions of constitutional supercooling, J. Crystal Growth **49**, 612–690 (1980)

4.45 J.E. Gegusin, A.S. Dziyuba: Gas evolution and the capture of gas bubbles a the crystallization front when growing crystals from the melt, Sov. Physics – Crystallogr. **22**, 197–199 (1977)

4.46 M. Göbbels: *Züchtung organischer Molekülkristalle aus entgasten unterkühlten Schmelzen*. Studienarbeit (Inst. f. Kristallographie, RWTH Aachen), in German

4.47 G. Engel, H. Klapper, P. Krempl, H. Mang: Growth-twinning in quartz-homeotypic gallium orthophosphate crystals, J. Crystal Growth **94**, 597–606 (1989)

4.48 I.L. Smolsky, A.E. Voloshin, N.P. Zaitseva, E.B. Rudneva, H. Klapper: X-ray topographic study of striation formation in layer growth of crystals from solution, Philosoph. Transactions: Math, Phys. Eng. Sci. **357**, 2631–2649 (1999)

4.49 T. Nishinaga, P. Ge, C. Huo, J. He, T. Nakamura: Melt growth of striation and etch-pit free GaSb under microgravity, J. Crystal Growth **174**, 96–100 (1997)

4.50 P. Dold: Czochralski growth of doped germanium with an applied rotating magnetic field, Cryst. Res. Technol. **38**, 659–668 (2003)

4.51 H. Scheel: Theoretical and experimental solutions of the striation problem. In: *Crystal Growth Technology*, ed. by H.J. Scheel, T. Fukuda (Wiley, New York 2003), Chap. 4

4.52 N. Herres, A.R. Lang: X-ray topography of natural beryl using synchroton and conventional sources, J. Appl. Cryst. **16**, 47–56 (1983)

4.53 H. Klapper: Röntgentopographische Untersuchungen von Gitterstörungen in Benzil-Einkristallen, J. Crystal Growth **10**, 13–25 (1971)

4.54 K. Maeda, A. Sonoda, H. Miki, Y. Asakuma, K. Fukui: Synergy of organic dyes for DKP crystal growth, Cryst. Res. Technol. **39**, 1006–1013 (2004)

4.55 I.L. Smol'skii, A.A. Chernov, G. Yu. Kutznetsov, V.F. Parvov, V.N. Rozhanskii: Vicinal sectoriality in growth sectors of {011} faces of ADP crystals, Sov. Phys. – Crystallogr. **30**, 563–567 (1985)

4.56 I.L.. Smol'skii, N.P. Zaitseva: Characteristic defects and imperfections in KDP crystals grown at high rates. In: *Growth of Crystals*, Vol. 19, ed. by E.I. Givargizov, S.A. Grinberg (Plenum Press, New York 1995) pp. 173–185

4.57 J.J. De Yoreo, T.A. Land, L.N. Rashkovich, T.A. Onischenko, J.D. Lee, O.V. Monovskii, N.P. Zaitseva: The effect of dislocation cores on growth hillock vicinality and normal growth rates of KDP {101} surfaces, J. Crystal Growth **182**, 442–460 (1997)

4.58 A.G. Shtukenberg, Y.O. Punin, E. Haegele, H. Klapper: On the origin of inhomogeneity of anomalous birefringence in mixed crystals: An example of alums, Phys. Chem. Minerals **28**, 665–674 (2001)

4.59 H. Klapper, R.A. Becker, D. Schmiemann, A. Faber: Growth-sector boundaries and growth-rate dispersion in potassium alum crystals, Cryst. Res. Technol. **37**, 747–757 (2002)

4.60 W.J.P. Van Enckevort, H. Klapper: Observation of growth steps with full and half unit-cell heights on the {001} faces of $NiSO_4.6H_2O$ in relation to the defect structure, J. Crystal Growth **80**, 91–103 (1987)

4.61 H. Kanda, M. Akaishi, S. Yamaoka: Impurity distribution among vicinal slopes of growth spirals developing on the {111} faces of synthetic diamonds, J. Crystal Growth **108**, 421–424 (1991)

4.62 J.J. De Yoreo, Z.U. Rek, N.P. Zaitseva, B.W. Woods: Sources of optical distortion in rapidly grown crystals of KH_2PO_4, J. Crystal Growth **166**, 291–297 (1996)

4.63 K. Fujioka, S. Matsuo, T. Kanabe, H. Fujita, M. Nakjatsuka: Optical properties of rapidly grown KDP crystals improved by thermal conditioning, J. Crystal Growth **181**, 265–271 (1997)

4.64 N. Zaitseva, L. Carman, I. Smolsky, R. Torres, M. Yan: The effect of impurities and supersaturation on the rapid growth of KDP crystals, J. Cryst. Growth **204**, 512–524 (1999)

4.65 T. Bullard, M. Kurimoto, S. Avagyan, S.H. Jang, B. Kahr: Luminescence imaging of growth hillocks in potassium hydrogen phthalate, ACA Trans. **39**, 62–72 (2004)

4.66 A.R. Lang, V.F. Miuskov: Dislocations and fault surfaces in synthetic quartz, J. Appl. Phys. **38**, 2477–2483 (1967), esp. p. 2482

4.67 A.R. Lang, V.F. Miuskov: Defects in natural and synthetic quartz. In: *Growth of Crystals*, Vol. 7, ed. by N.N. Sheftal (Consultants Bureau, New York 1969) pp. 112–123, esp. p. 122

4.68 W. Schmidt, R. Weiss: Dislocation propagation in Czochralski grown gadolinium gallium garnet, J. Crystal Growth **43**, 515–525 (1978)

4.69 B. Cockayne, J.M. Roslington, A.W. Vere: Microscopic strain in facetted regions of garnet crystals, J. Mat. Sci. **8**, 382–384 (1973)

4.70 W.T. Stacy: Dislocations, facet regions and grown striations in garnet substrates and layers, J. Crystal Growth **24/25**, 137–143 (1974)

4.71 T. Hahn, H. Klapper: Twinning of crystals. In: *International Tables for Crystallography*, Vol. D (Kluwer Academic Publishers, Dordrecht 2003) pp. 393–448

4.72 A. Shtukenberg, Y. Punin, B. Kahr: Optically anomalous crystals. In: *Springer Series in Solid State Science* (Springer, Berlin, Heidelberg 2007)

4.73 R. von Brauns: *Die optischen Anomalien der Krystalle* (S. Hirzel, Leipzig 1891)

4.74 B. Kahr, J.M. McBride: Optically anomalous crystals, Angew. Chem. Internat. Edn. **31**, 1–26 (1992)

4.75 H. Klapper: Reconstruction of the growth history of crystals by analysis of growth defects. In: *Crystal Growth of Technologically Important Electronic Materials*, ed. by K. Byrappa, T. Ohachi, H. Klapper, R. Fornari (Allied Publishers PVT. Ltd, 2003)

4.76 J.N. Sherwood, T. Shiripathi: Evidence for the role of pure edge dislocations in crystal growth, J. Crystal Growth **88**, 358–364 (1988)

4.77 H.L. Bhat, R.I. Ristic, J.N. Sherwood, T. Shiripathi: Dislocation characterization in crystal of potash alum grown by seeded solution growth und conditions of low supersaturation, J. Crystal Growth **121**, 709–716 (1992)

4.78 R.I. Ristic, B. Shekunov, J.N. Sherwood: Long and short period growth rate variations in potash alum, J. Crystal Growth **160**, 330–336 (1996)

4.79 E. Billig: Some defects in crystals grown from the melt I: Defects caused by thermal stresses, Proc. Royal Soc. London (A) **235**, 37–55 (1956)

4.80 V.L. Indenbom: Ein Beitrag zur Entstehung von Spannungen und Versetzungen beim Kristallwachstum, Kristall und Technik **14**, 493–507 (1979), in German

4.81 P. Möck: Comparison of experiments and theories for plastic deformation in thermally processed GaAs wafers, Cryst. Res. Technol. **35**, 529–540 (2000)

4.82 P. Rudolph: Dislocation cell structures in melt-grown semiconductor compound crystals, Cryst. Res. Technol. **40**, 7–20 (2005)

4.83 Y.M. Fishman: X-ray topographic study of the dislocations produced in potassium dihydrogen phosphate crystals by growth from solution, Sov. Physics – Cryst. **17**, 524–527 (1972)

4.84 G. Dhanaraj, M. Dudley, D. Bliss, M. Callahan, M. Harris: Growth and process induced dislocations in zinc oxide crystals, J. Crystal Growth **297**, 74–79 (2006)

4.85 G. Neuroth: Der Einfluß von Einschlussbildung und mechanischer Verletzung auf das Wachstum und

die Perfektion von Kristallen. Ph.D. Thesis (Shaker Verlag, Aachen 1996), University of Bonn, 1996, in German
4.86 A.J. Forty: Direct observation of dislocations in crystals, Adv. Phys. **3**, 1–25 (1954)
4.87 G.G. Lemmlein, E.D. Dukova: Formation of screw dislocation in the growth process of a crystal, Sov. Phys. – Crystallogr. **1**, 269–273 (1956)
4.88 M.I. Kozlovskii: Formation of screw dislocations in the growth of a crystal around solid particles, Sov. Phys. – Crystallogr. **3**, 205–211 (1958/60)
4.89 M.I. Kozlovskii: Formation of screw dislocations at the junction of two layers spreading over the surface of a crystal, Sov. Phys. – Crystallogr. **3**, 236–238 (1958/60)
4.90 M. Dudley, X.R. Huang, W. Huang, A. Powell, S. Wang, P. Neudeck, M. Skowronski: The mechanism of micropipe nucleation at inclusions in silicon carbide, Appl. Phys. Lett. **75**, 784–786 (1999)
4.91 W.T. Read: *Dislocations in Crystals* (McGraw-Hill, New York 1953) p. 47
4.92 D. Hull: *Introduction to Dislocations* (Pergamon Press, Oxford 1975) pp. 229–235, 2nd edn.
4.93 J.P. Hirth, J. Lothe: *Theory of Dislocations* (McGraw-Hill, New York 1968)
4.94 H. Klapper: Vorzugsrichtungen eingewachsener Versetzungen in lösungsgezüchteten Kristallen. Habilitation Thesis, (Technical University (RWTH) Aachen 1975), in German
4.95 J. Lothe: Force on dislocations emerging at free surfaces, Physica Norvegica **2**, 154–157 (1967)
4.96 J.B. Eshelby, W.T. Read, W. Shockley: Anisotropic elasticity with applications to dislocation theory, Acta Metall. **1**, 251–259 (1953)
4.97 H. Klapper, M. Yu. Fishman, V.G. Lutsau: Elastic energy and line directions of grown-in dislocations in KDP crystals, Phys. Stat. Sol. (a) **21**, 115–121 (1974)
4.98 H. Klapper: Elastische Energie und Vorzugsrichtungen geradliniger Versetzungen in aus der Lösung gewachsenen organischen Kristallen. I. Benzil, Phys. Stat. Sol. (a) **14**, 99–106 (1972), in German
4.99 H. Klapper: Elastische Energie und Vorzugsrichtungen geradliniger Versetzungen in aus der Lösung gewachsenen organischen Kristallen. II. Thioharnstoff, Phys. Stat. Sol. (a) **14**, 443–451 (1972), in German
4.100 H. Klapper: Röntgentopographische Untersuchungen am Lithiumformiat-Monohydrat, Z. Naturforsch. **28a**, 614–622 (1973), in German
4.101 H. Klapper, H. Küppers: Directions of dislocation lines in crystals of ammonium hydrogen oxalate hemihydrate grown from solution, Acta Cryst. **A29**, 495–503 (1973), (correction: read $K/\cos\alpha$ instead of $K\cos\alpha$)
4.102 D.F. Croxall, R.C.C. Ward, C.A. Wallace, R.C. Kell: Hydrothermal growth and investigation of Li-doped zinc oxide crystals of high purity and perfection, J. Crystal Growth **22**, 117–124 (1974)
4.103 U. Alter, G. Voigt: Direction change of dislocations on passing a growth-sector boundary in quartz crystals, Cryst. Res. Technol. **19**, 1619–1623 (1984)
4.104 K. Izumi: Lattice defects in normal alcohol crystals, Jap. J. Appl. Phys. **16**, 2103–2108 (1977)
4.105 A. Sakai, H. Sunakawa, A. Usui: Defect structure in selectively grown GaN films with low threading dislocation density, Appl. Phys. Lett. **71**, 2259–2261 (1997)
4.106 Z. Liliental-Weber, M. Benamara, W. Snider, J. Washburn, J. Park, P.A. Grudowski, C.J. Eiting, R.D. Dupuis: TEM study of defects in laterally overgrown GaN layers, MRS Internet J. Nitride Semicond. Res. **4s1**, 4.6 (1999)
4.107 H. Sunakawa, A. Kimura, A. Usui: Self-organized propagation of dislocations in GaN films during epitaxial lateral overgrowth, Appl. Phys. Lett. **76**, 442–444 (2000)
4.108 P. Venégues, B. Beaumont, V. Bousquet, M. Vaille, P. Gibart: Reduction mechanisms of defect densities in GaN using one- or two-step epitaxial lateral overgrowth methods, J. Appl. Phys. **87**, 4175–4181 (2000)
4.109 S. Gradezcak, P. Stadelman, V. Wagner, M. Ilegems: Bending of dislocations in GaN during epitaxial lateral overgrowth, Appl. Phys. Lett. **85**, 4648–4650 (2004)
4.110 J. Bai, J.-S. Park, Z. Cheng, M. Curtin, B. Adekore, M. Carroll, A. Lochtefeld, M. Dudley: Study of the defect elimination mechanism in aspect ratio trapping Ge growth, Appl. Phys. Lett. **80**, 10192 (2007)
4.111 N. Zaitseva, L. Carman, I. Smolsky: Habit control during rapid growth of KDP and DKDP crystals, J. Crystal Growth **241**, 363–373 (2002)
4.112 G.R. Ester, P.J. Halfpenny: An investigation of growth-induced defects in crystals of potassium hydrogen phthalate, Phil. Mag. A **79**, 593–608 (1999)
4.113 G.R. Ester, R. Price, P.J. Halfpenny: The relationship between crystal growth and defect structure: a study of potassium hydrogen phthalate using X-ray topography and atomic force microscopy, J. Phys. D: Appl. Phys. **32**, A128–A132 (1999)
4.114 J. Weertmann, J.R. Weertmann: *Elementary Dislocation Theory* (The Macmillan Company, New York 1964) p. 137
4.115 I.L. Smolsky, E.B. Rudneva: Effect of the surface morphology on the grown-in dislocation orientations in KDP crystals, Phys. Stat. Sol. (a) **141**, 99–107 (1994)
4.116 G. Neuroth, H. Klapper: Dislocation reactions in Czochralski-grown salol crystals, Z. Kristallogr. **209**, 216–220 (1994)
4.117 T. Watanabe, K. Izumi: Growth and perfection of tetraoxane crystals, J. Crystal Growth **46**, 747–756 (1979)
4.118 H. Klapper: Röntgentopographische Untersuchungen der Defektstrukturen im Thioharnstoff, J. Crystal Growth **15**, 281–287 (1972), in German

4.119 F.C. Frank: The influence of dislocations on crystal growth, Disc. Faraday Soc. **5**, 48–54 (1949), and 66–68

4.120 C.F. Frank: Crystal growth and dislocations, Adv. Phys. **1**, 91–109 (1952)

4.121 W.K. Burton, N. Cabrera, F.C. Frank: The growth of crystals and the equilibrium structure of their surfaces, Phil. Trans. Roy. Soc. London A **243**, 299–358 (1951), especially Part II, pp. 310–323

4.122 H.P. Strunk: Edge dislocation may cause growth spirals, J. Crystal Growth **160**, 184–185 (1996)

4.123 N.-B. Ming: Defect mechanism of crystal growth and their kinetics, J. Crystal Growth **128**, 104–112 (1993)

4.124 E. Bauser, H. Strunk: Analysis of dislocations creating monomolecular growth steps, J. Crystal Growth **51**, 362–366 (1981)

4.125 F.C. Frank: "Edge" dislocations as crystal growth sources, J. Crystal Growth **51**, 367–368 (1981)

4.126 L.J. Giling, B. Dam: A "rough heart" model for "edge" dislocations which act as persistent growth sources, J. Crystal Growth **67**, 400–403 (1984)

4.127 H. Gottschalk, G. Patzer, H. Alexander: Stacking-fault energy and ionicity of cubic III-V compounds, Phys. Status Solidi A **45**, 207–217 (1978)

4.128 T.W. Donnelly: Kinetic considerations in the genesis of growth twinning, Amer. Mineralogist **52**, 1–12 (1967)

4.129 H. Carstens: Kinetic consideration in the genesis of growth twinning: A discussion, Amer. Mineralogist **53**, 342–344 (1968), ;

4.130 T.W. Donnelly: Kinetic consideration in the genesis of growth twins: A reply, Amer. Mineralogist **53**, 344–346 (1968)

4.131 V. Janovec, T. Hahn, H. Klapper: Twinning and domain structures. In: *International Tables for Crystallography* (Kluwer Academic Publishers, Dordrecht 2003) p. 377–378, Vol. D

4.132 V. Janovec, J. Přívratská: Domain structures. In: *International Tables for Crystallography*, Vol. D (Kluwer Academic Publishers, Dordrecht 2003) pp. 449–505

4.133 F.D. Bloss: *Crystallography and Crystal Chemistry* (Rinehart & Winston, New York 1971) pp. 324–338

4.134 C. Giacovazzo (ed.): *Fundamentals of Crystallography* (University Press, Oxford 1992) pp. 80–87, and 133–140

4.135 C. Frondel: Silica minerals. In: *The System of Mineralogy*, 7th edn., Vol. III, (Wiley, New York 1962) pp. 75–99

4.136 J.W. Faust Jr., H.F. John: The growth of semiconductor crystals from solution using the twin-plane reentrant-edge mechanism, J. Phys. Chem. Solids **25**, 1407–1415 (1964)

4.137 R. Jagannathan, R.V. Mehta, J.A. Timmons, D.L. Black: Anisotropic growth of twinned cubic crystals, Phys. Rev. B **48**, 13261–13265 (1993)

4.138 R. Jagannathan, R.V. Mehta, J.A. Timmons, D.L. Black: Reply to comment on anisotropic growth of twinned cubic crystals, Phys. Rev. B **51**, 8655 (1995), following the Comment by B.W. van de Waal, Phys. Rev. B **51**, 8653–8654 (1995)

4.139 G. Bögels, T.M. Pot, H. Meekes, P. Bennema, D. Bollen: Side-face structure for lateral growth of tabular silver bromide crystals, Acta Cryst. A **53**, 84–94 (1997)

4.140 G. Bögels, H. Meekes, P. Bennema, D. Bollen: The role of {100} side faces for lateral growth of tabular silver bromide crystals, J. Crystal Growth **191**, 446–456 (1998)

4.141 G. Bögels, J.G. Buijnsters, S.A.C. Verhaegen, H. Meekes, P. Bennema, D. Bollen: Morphology and growth mechanism of multiply twinned AgBr and AgCl needle crystals, J. Crystal Growth **203**, 554–563 (1999)

4.142 C.A. Wallace, E.A.D. White: The morphology and twinning of solution-grown corundum crystals. In: *Crystal Growth*, ed. by H.S. Peiser (Pergamon Press, Oxford 1967) pp. 431–435, supplement to Phys. Chem. Solids

4.143 M. Senechal: The genesis of growth twins, Sov. Phys. – Crystallogr. **25**, 520–524 (1980)

4.144 H. Hofmeister: Forty years study of fivefold twinned structures in small particles and thin films, Cryst. Res. Technol. **33**, 3–25 (1998), especially Section 4

4.145 I. Sunagawa, L. Taijing, V.S. Balitsky: Generation of Brazil and Dauphiné twins in synthetic amethyst, Phys. Chem. Minerals **17**, 320–325 (1990)

4.146 A.C. MacLaren, D.R. Pitkethly: The twinning microstructure and growth of amethyst quartz, Phys. Chem. Minerals **8**, 128–135 (1982)

4.147 H. Klapper, T. Hahn, S.J. Chung: Optical, pyroelectric and X-ray topographic studies of twin domains and twin boundaries in $KLiSO_4$, Acta Cryst. B **43**, 147–159 (1987)

4.148 M.J. Buerger: The genesis of twin crystals, Am. Mineralogist **30**, 469–482 (1945)

4.149 P. Hartmann: On the morphology of growth twins, Z. Kristallogr. **107**, 225–237 (1956)

4.150 R. Docherty, A. El-Korashi, H.-D. Jennissen, H. Klapper, K.J. Roberts, T. Scheffen-Lauenroth: Synchroton Laue topographic studies of pseudo-hexagonal twinning, J. Appl. Cryst. **21**, 406–415 (1988)

4.151 N.-B. Ming, I. Sunagawa: Twin lamellae as possible self-perpetuating steps sources, J. Crystal Growth **87**, 13–17 (1988), ;

4.152 N.-B. Ming, K. Tsukamato, I. Sunagawa, A.A. Chernov: Stacking faults as self-perpetuating step sources, J. Crystal Growth **91**, 11–19 (1988)

4.153 H. Li, X.-D. Peng, N.-B. Ming: Re-entrant corner mechanism of fcc crystal growth of A-type twin lamella: the Monte-Carlo simulation approach, J. Crystal Growth **139**, 129–133 (1994)

4.154 H. Li, N.-B. Ming: Growth mechanism and kinetics on re-entrant corner and twin lamellae in a fcc crystal, J. Crystal Growth **152**, 228–234 (1995)

4.155 R.-W. Lee, U.-J. Chung, N.M. Hsang, D.-Y. Kim: Growth process of the ridge-trough faces of a twinned crystal, Acta Cryst. A **61**, 405–410 (2005)
4.156 R. Boistelle, D. Aquilano: Interaction energies at twin boundaries and effects of the dihedral re-entrant and salient angles on the grown morphology of twinned crystals, Acta Cryst. A **34**, 406–413 (1978)
4.157 I.M. Dawson: The study of crystal growth with the electron microscope II. The observation of growth steps in the paraffin n-hexane, Proc. Roy. Soc. London A **214**, 72–79 (1952)
4.158 R.S. Wagner: On the growth of Ge dendrites, Acta Metal. **8**, 57–60 (1960)
4.159 D.R. Hamilton, R.G. Seidensticker: Propagation mechanism of germanium dendrites, J. Appl. Phys. **31**, 1165–1168 (1960)
4.160 B. van de Waal: Cross-twinning model of fcc crystal growth, J. Crystal Growth **158**, 153–165 (1996)
4.161 G. Roth, D. Ewert, G. Heger, M. Hervieu, C. Michel, B. Raveau, B. D'Yvoire, A. Revcolevschi: Phase transformation and microtwinning in crystals of the high-Tc superconductor $YBa_2Cu_3O_{8-x}$, Z. Physik B **69**, 21–27 (1987)
4.162 I.S. Zheludev: Crystallography and spontaneous polarisation. In: *Physics of Crystalline Dielectrics*, Vol 1 (Plenum Press, New York 1971)
4.163 M. Nakatsuka, K. Fujioka, T. Kanabe, H. Fujita: Rapid growth of over 50 mm/day of water-soluble KDP crystal, J. Crystal Growth **171**, 531–537 (1997)
4.164 H. Klapper, I.L. Smolsky, A.E. Haegele: Rapid growth from solution. In: *Crystal Growth of Technologically Important Electronic Materials*, ed. by K. Byrappa, T. Ohachi, H. Klapper, R. Fornari (Allied Publishers PVT. Ltd, 2003)

http://www.springer.com/978-3-540-74182-4

Springer Handbook of Crystal Growth
(Eds.)G. Dhanaraj; K. Byrappa; V. Prasad; M. Dudley
2010, XXXVIII, 1818 p. 1251 illus. in color. With DVD.,
Hardcover
ISBN: 978-3-540-74182-4